Myosin Vs organize actin cables in fission yeast

Libera Lo Presti[a], Fred Chang[b], and Sophie G. Martin[a]
[a]Department of Fundamental Microbiology, Faculty of Biology and Medicine, University of Lausanne, CH-1015 Lausanne, Switzerland; [b]Department of Microbiology, College of Physicians and Surgeons, Columbia University, New York, NY 10032

ABSTRACT **Myosin V motors are believed to contribute to cell polarization by carrying cargoes along actin tracks. In *Schizosaccharomyces pombe*, Myosin Vs transport secretory vesicles along actin cables, which are dynamic actin bundles assembled by the formin For3 at cell poles. How these flexible structures are able to extend longitudinally in the cell through the dense cytoplasm is unknown. Here we show that in myosin V (*myo52 myo51*) null cells, actin cables are curled, bundled, and fail to extend into the cell interior. They also exhibit reduced retrograde flow, suggesting that formin-mediated actin assembly is impaired. Myo52 may contribute to actin cable organization by delivering actin regulators to cell poles, as *myoV*Δ defects are partially suppressed by diverting cargoes toward cell tips onto microtubules with a kinesin 7–Myo52 tail chimera. In addition, Myo52 motor activity may pull on cables to provide the tension necessary for their extension and efficient assembly, as artificially tethering actin cables to the nuclear envelope via a Myo52 motor domain restores actin cable extension and retrograde flow in *myoV* mutants. Together these in vivo data reveal elements of a self-organizing system in which the motors shape their own tracks by transporting cargoes and exerting physical pulling forces.**

Monitoring Editor
Laurent Blanchoin
CEA Grenoble

Received: Jul 5, 2012
Revised: Sep 5, 2012
Accepted: Oct 3, 2012

INTRODUCTION

F-actin and microtubules support cell architecture and function, in part by forming tracks for the polarized trafficking of signaling molecules and organelles (Brennwald and Rossi, 2007; Chesarone *et al.*, 2011). Efficient trafficking depends on the activity of motor proteins and their interaction with cargoes, as well as on the organization and accessibility of the tracks.

The actin cytoskeleton is organized by a host of actin-binding proteins (ABPs), which function to nucleate, elongate, cross-link, and sever filaments. Actin filaments serve as tracks for myosin motors, of which up to 30 distinct classes have been identified from yeast to higher eukaryotes (Woolner and Bement, 2009). Although the best-described functions of myosins lie in cargo and organelle transport and force generation, evidence in many organisms indicates that myosins are not simple users of the actin tracks but also contribute to their organization (Woolner and Bement, 2009; Reymann *et al.*, 2012). For instance, conventional type II myosin promotes the retrograde flow of actin cables through the bud neck of *Saccharomyces cerevisiae* (Huckaba *et al.*, 2006). In mammalian cells unconventional myosin X motor activity promotes actin convergence for filopodia formation (Berg and Cheney, 2002; Bohil *et al.*, 2006).

Even myosin V, the prototypical transport myosin specialized in the directed transport of cargoes toward actin filament barbed ends (Hammer and Sellers, 2012), may contribute to the architecture of the actin cytoskeleton. Myosin V regulates the motility of actin cables along the cortex of unpolarized budding yeast cells (Yu *et al.*, 2011), and some evidence suggests a role in actin cytoskeleton organization in mammalian cells (Eppinga *et al.*, 2008). These motor proteins are composed of an N-terminal motor domain with F-actin and ATP-binding sites, a lever arm rich in IQ repeats with regulatory function, a coil-coiled domain that allows dimerization, and a globular tail that mediates cargo binding (Li and Nebenfuhr, 2008; Trybus, 2008).

Fission yeast is a rod-shaped unicellular organism that grows by polar extension at both cell poles. Polarized growth requires the

This article was published online ahead of print in MBoC in Press (http://www.molbiolcell.org/cgi/doi/10.1091/mbc.E12-07-0499) on October 10, 2012.

Address correspondence to: Sophie G. Martin (Sophie.Martin@unil.ch).

Abbreviations used: ABPs, actin-binding proteins; CHD, calponin-homology domain; CFP, cyan fluorescent protein; DMSO, dimethyl sulfoxide; EMM, Edinburgh minimal medium; FRAP, fluorescence recovery after photobleaching; GFP, green fluorescent protein; LatA, latrunculin A; MBC, methylbenzimidazole-2-yl-carbamate; myoV, myosin V; tdTomato, tandem dimeric Tomato; YFP, yellow fluorescent protein

transport and tethering of exocytic vesicles carrying cell wall–remodeling enzymes to cell poles (Bendezu and Martin, 2011). The myosin V Myo52 transports exocytic vesicles along actin cables toward cell poles by binding a cargo receptor, the Rab11-like GTPase Ypt3 (Lo Presti and Martin, 2011). Accordingly, *myo52* mutant cells are misshapen and display severe growth defects, underlying the function of Myo52 in vesicle delivery to zones of growth (Motegi *et al.*, 2001; Win *et al.*, 2001; Mulvihill *et al.*, 2006; Grallert *et al.*, 2007). Fission yeast encodes a second type V myosin, Myo51, which has roles during sexual reproduction but no reported function during vegetative growth (Win *et al.*, 2001; Doyle *et al.*, 2009).

The assembly and dynamics of actin cables in yeasts resemble those of actin structures within filopodia, microvilli, and stereocilia in metazoa. All these structures are formed by actin bundles composed of short actin filaments mostly oriented with their barbed ends toward the cell membrane (Kamasaki *et al.*, 2005). Each filament within the bundle is believed to be nucleated at the plasma membrane by formins, stabilized by tropomyosin, bundled, and likely disassembled in the cytoplasm (Moseley and Goode, 2006; Nambiar *et al.*, 2010). Time-lapse imaging shows that the actin cables in yeasts undergo retrograde flow (Martin and Chang, 2006; Buttery *et al.*, 2007). Dots of formin reside transiently at the plasma membrane, where they assemble actin filaments that may push the whole actin bundle into the cell interior. Formin dots are then released and move in a directed manner away from the cell tip, probably associated with the barbed ends of actin filaments in the bundle. In the fission yeast, For3 is the formin responsible for actin cable assembly (Feierbach and Chang, 2001; Nakano *et al.*, 2002). How these flexible structures are able to extend through a dense cytoplasm has not been clear. Here we show that myosin Vs contribute to the organization and dynamics of actin cables, suggesting that motors and cables form a self-organizing system in which the motor shapes its own tracks.

RESULTS

Class V myosins are required for the extension of actin cables

We analyzed the actin cable organization of cells lacking one or both type V myosins in fixed cells by staining them with Alexa Fluor–phalloidin and in live cells by imaging the F-actin marker green fluorescent protein (GFP)–CHD_{Rng2} (calponin-homology domain; Karagiannis *et al.*, 2005). In interphase, wild-type and *myo51*Δ cells display straight actin cables running from the tips throughout the entire length of the cell, as well as actin patches polarized at tips. In contrast, *myo52*Δ and to a greater extent *myo52*Δ *myo51*Δ (here labeled as *myoV*Δ) cells exhibit, in addition to the previously described depolarization of actin patches (Motegi *et al.*, 2001), short, curly, misoriented cables, which do not span the entire cell length and often converge from the cell tip into a single thick bundle (Figure 1, A–C). We quantified this defect by counting the proportion of cells displaying 1) at least one cable oriented in a direction distinct from the longitudinal axis of cell, 2) a thick bundle, or 3) fewer than three cables extending across the middle of the cell (Figure 1B). Time-lapse imaging further revealed how these thick cables fail to extend into the cell and instead exhibit wavy movements at cell tips (Supplemental Movies S1 and S2). Thus myosin Vs are required for actin cable extension through the cell. Of note, mutant cells expressing the GFP-CHD_{Rng2} marker exhibited more pronounced actin defects than those seen in phalloidin-stained cells, probably due to the actin-bundling properties of the CHD itself (Takaine *et al.*, 2009). However even upon 24-h induction of GFP-CHD_{Rng2} expression, which caused extensive actin cable tangling, wild-type cells never displayed the *myoV*Δ cable phenotype described (unpublished data).

We considered the possibility that this actin defect might be a consequence of abnormal cell morphology. Three lines of evidence excluded it. First, although *myo52*Δ and *myoV*Δ cells have similar cell shapes (Motegi *et al.*, 2001; Win *et al.*, 2001), only *myoV*Δ displays severe actin cable defects. Second, other round mutants, such as *orb2-34* or *orb6-25* mutant, which have a disorganized actin cytoskeleton, did not show curly and thicker cables (Verde *et al.*, 1995; Figure 1D). Third, we combined the *myoV* deletions with *cdc25-22* to produce elongated cells due to cell cycle delay: *myoV*Δ *cdc25-22* cells were more elongated than *myoV*Δ cells but still displayed the cable organization defect (>95% of cells showed misoriented and thick cables, and >70% of cells showed an extension defect, $n = 27$; Figure 1E). We conclude that the defect in actin cable organization observed in *myoV* mutants is not a consequence of abnormal cell morphology.

We also considered the possibility that the actin cable defect may be a consequence of microtubule disruption, as microtubules are disorganized in *myoV*Δ cells (Lo Presti and Martin, 2011). However, disruption of microtubules by treatment with methyl-benzidazole-carbamate (MBC) for 30 min in wild-type cells or by deletion of *mal3*, encoding the EB1 homologue, in which microtubules are short and unstable (Beinhauer *et al.*, 1997), did not cause important actin cable abnormalities (Supplemental Figure S1). In contrast, MBC treatment of *myoV*Δ cells consistently led to a worsening of the cable phenotype (Supplemental Figure S1). Similarly, combining *myoV*Δ with *mal3*Δ led to a stronger cable phenotype than that of *myoV*Δ (Supplemental Figure S1). These data indicate that microtubules likely play a role in actin cable organization, not investigated further here, but which is revealed only upon deletion of myosin Vs. Thus the actin cable defect observed in *myoV*Δ cells is not a consequence of microtubule disruption.

To quantify the retrograde flow of actin in cables, we monitored the formin For3 using a functional For3-3GFP fusion. For3 localizes to dots at cell tips, which detach from the cortex and move toward the cell interior together with the actin filaments in the cable (Martin and Chang, 2006). For3 dots thus serve as marks for the retrograde movement of actin in the cell. For3-3GFP localized correctly to cell tips in cells lacking both *myo52* and *myo51* (Figure 2A), suggesting that cable misorganization is not due to gross defects in formin localization. However, these cells displayed a decrease in For3 retrograde movements: in *myoV*Δ cells, For3-3GFP dots moved inward at a rate of 0.16 ± 0.09 μm/s ($n = 128$), about half the wild-type rate of 0.31 ± 0.13 μm/s ($n = 112$; *t* test $p = 2e^{-20}$; Figure 2, B and C, and Supplemental Movies S3 and S4). Cells lacking either *myo52* or *myo51* displayed only a mild decrease in retrograde flow, with average values of 0.28 ± 0.11 μm/s ($n = 78$, *t* test $p > 0.05$) and 0.25 ± 0.10 μm/s ($n = 109$, *t* test $p = 0.002$), respectively. Consistent with this slower For3 retrograde flow, For3 turnover at cell tips was reduced in *myoV*Δ cells, as assessed by fluorescence recovery after photobleaching (FRAP) analysis, with recovery half-time of ~20 s compared with ~10 s in wild-type cells (Figure 2D). Thus myosin Vs contribute to the organization and retrograde flow of actin cables.

Myo52 requires its cargo-binding tail for cable organization

To start dissecting the role of cargoes in myosin Vs in cable organization, we generated truncated tagged alleles that lacked the predicted cargo-binding C-terminal tail but retained the coiled-coil dimerization domain and expressed them as unique copies under their endogenous promoter. Like the full-length protein, Myo52Δtail-tdTomato localized to cell poles in wild-type and *myo51*Δ cells,

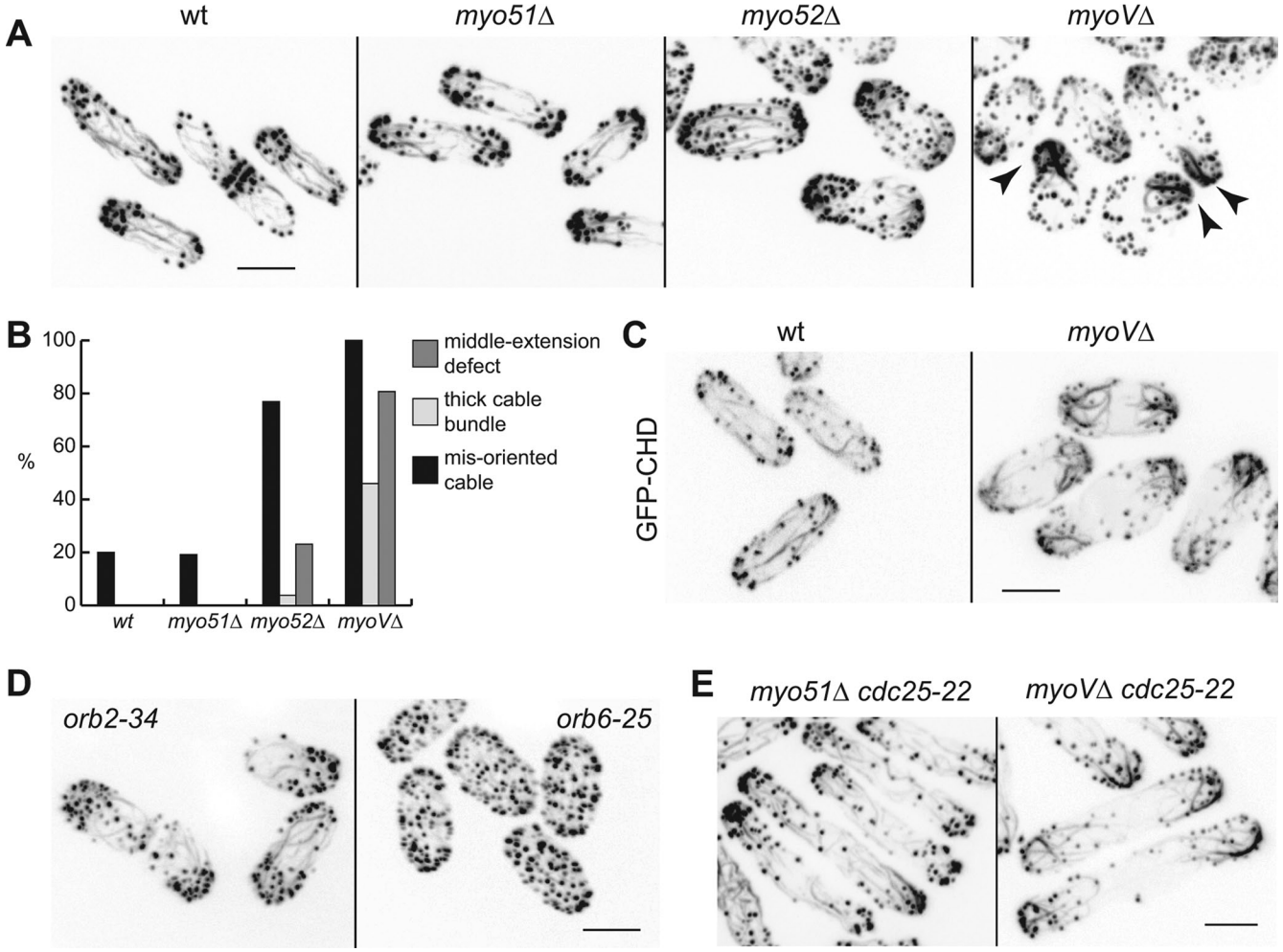

FIGURE 1: *myoV*-null cells display aberrant actin cable organization. (A) Alexa Fluor–phalloidin staining of wild-type (wt), *myo51*Δ, *myo52*Δ, and *myo51*Δ*myo52*Δ (*myoV*Δ) cells. Arrowheads point to misoriented and thicker cables in mutant cells. (B) Quantification of the actin defect (see *Materials and Methods*). (C) Actin organization in live cells expressing the actin marker GFP-CHD_{Rng2} (see Supplemental Movies S1 and S2). (D) Alexa Fluor–phalloidin staining of *orb2-34* or *orb6-25* cells. Cells were grown at permissive temperature (25°C) for 14 h and fixed after 2-h shift to restrictive temperature (36°C) to induce round morphology. (E) Alexa Fluor–phalloidin staining of *cdc25-22 myo51*Δ and *cdc25-22 myoV*Δ cells grown at permissive temperature (25°C) for 14 h and fixed after 2-h shift to semipermissive temperature (30°C) to enhance cell elongation. Inverted images are shown throughout. Scale bars, 5 μm.

suggesting that this allele retained motor activity (Figure 3A). This localization was actin cable dependent, as cell tip localization was abolished in *for3*Δ or by treatment with low latrunculin A (LatA) dose (10 μM), which disrupts actin cables but not patches (Figure 3A). We note that Myo52Δtail, like full-length Myo52, still localized to the division site in the absence of actin cables (Figure 3A). We note also that Myo52Δtail-tdTomato did not form discrete dots like the full-length protein, suggesting loss of motor–cargo interaction. *myo52Δtail-tdTomato* cells were as sick and misshapen as *myo52*Δ cells, again suggesting that interaction with cargoes important for polarized growth was impaired. Fluorescence measurements indicated somewhat lower levels of expression compared with full-length Myo52-tdTomato (twofold lower; Supplemental Figure S2C) in wild-type, *myo51*Δ, and *for3*Δ *myo51*Δ cells, suggesting that this truncated allele may be unstable. *myo52Δtail myo51*Δ cells were as defective as *myoV*Δ cells for actin cable organization (Figure 3, B and E, and unpublished data), and for retrograde flow (*myo52Δtail-tdTomato myo51*Δ rate, 0.158 ± 0.078 μm/s, $n = 93$; Figure 3F). These results suggest that Myo52 requires its tail for actin cable organization.

The only known cargo receptor for Myo52, the essential Rab11-family GTPase Ypt3 (Lo Presti and Martin, 2011), plays multiple functions in the secretory pathway (Cheng *et al.*, 2002; He *et al.*, 2006). Whereas the hypomorphic allele *ypt3-i5* showed highly aberrant actin organization at the restrictive temperature of 36°C (unpublished data), at the permissive temperature (25°C) *ypt3-i5* mutants showed defects consistent with a function in cable organization. Fixed and time-lapse live imaging showed thick, curly actin cables in *ypt3-i5 myo51*Δ cells, but the phenotype was much milder than in *myo52Δtail myo51*Δ cells (Supplemental Figure S3, A–C). In these conditions, Myo52-tdTomato localized correctly at cell tips but did not form discrete dots in the cytoplasm (Supplemental Figure S3D). This suggests that Myo52–Ypt3 interactions may be lost in this mutant but that the myosin is still able to bind and move on cables, in contrast to what was observed for Myo2p in budding yeast (Lipatova *et al.*, 2008). The mild defect may indicate residual Ypt3 activity and/or the existence of additional Myo52 cargoes for cable organization, as also shown by the polarized shape of *ypt3-i5* cells at 25°C. Taken together, these data indicate that Myo52 requires cargo binding to organize actin cables.

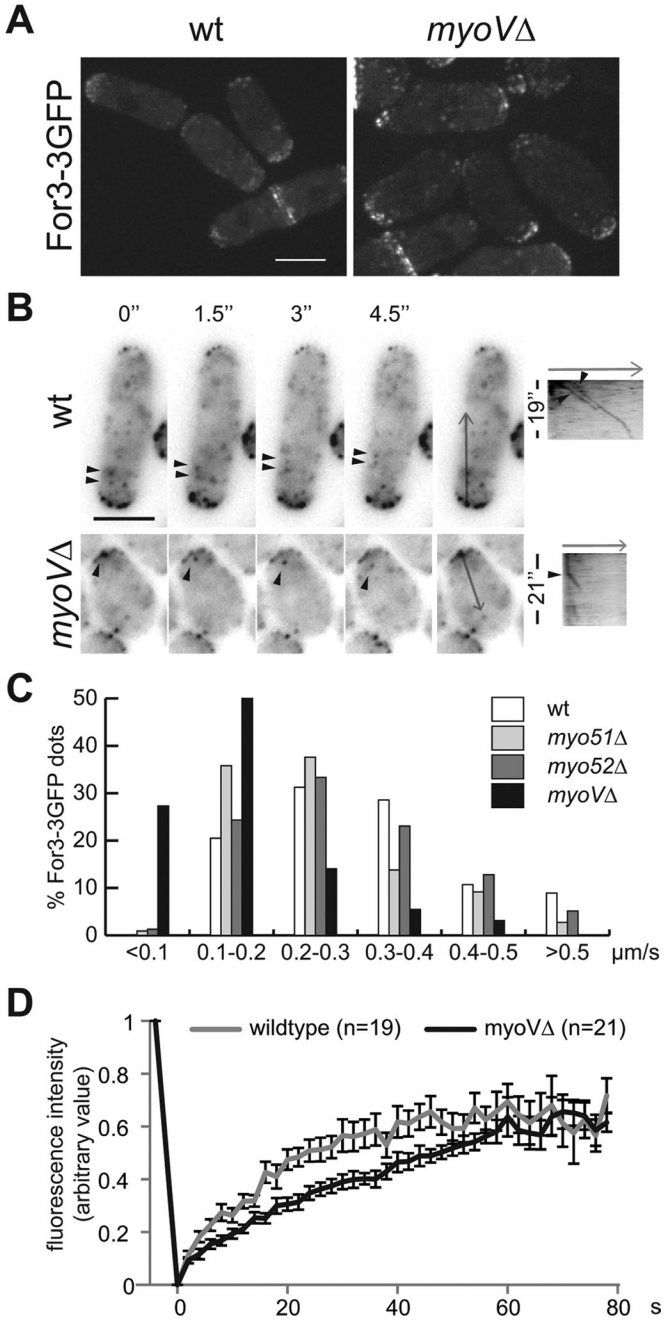

FIGURE 2: *myoV*-null cells exhibit a decrease in F-actin retrograde flow rate. (A) Maximum-intensity projection images of wild-type (left) and *myoV*Δ (right) cells expressing For3-3GFP. (B) Inverted time-lapse images (single focal plane) and corresponding kymographs of For3-GFP in wild-type and *myoV*Δ cells (see Supplemental Movies S3 and S4). Arrowheads point to retrograde movements. (C) Histogram distribution of retrograde For3p-3GFP dot rates. (D) Quantification of the FRAP of For3-3GFP in wild-type and *myoV*Δ. Each trace represents the average value for the indicated number of experiments. Error bars, SEM. The data from wild type are identical to that shown in Martin and Chang (2006). Scale bars, 5 μm.

Myo51 does not require its cargo-binding tail for cable organization

No function or localization had previously been detected for Myo51 in vegetative growing cells (Motegi *et al.*, 2001; Win *et al.*, 2001). However, the aforementioned data suggested that Myo51 is involved in cable organization. We thus reinvestigated its localization: Myo51-GFP and Myo51–3 yellow fluorescent protein (YFP) labeled cable-like structures in wild-type interphase cells, a localization even more prominent in *myo52*Δ cells (Figure 3C and unpublished data). Myo51 also localized to rings in mitotic cells, as previously observed (Win *et al.*, 2001). Complete actin cytoskeleton disruption with 200 μM LatA abolished the cable-like signal of Myo51-3YFP. Specific actin cable disruption with 10 μM LatA or in *for3*Δ cells led to relocalization of Myo51 to actin patches, as shown by colocalization with the actin patch component Crn1 (Figure 3C and Supplemental Figure S2, A and B). Hence Myo51 binds actin and decorates actin cables.

Myo51Δtail-3GFP localized similarly to full-length Myo51-3YFP, decorating actin cables and rings in both wild-type and *myo52*Δ cells and localizing to actin patches and rings in *for3*Δ cells (Figure 3C), although it failed to localize to actin patches when cells were treated with 10 μM LatA, suggesting that its actin-binding properties may be slightly different (Supplemental Figure S2A). Surprisingly, Myo51Δtail was nearly as efficient as wild-type Myo51 in organizing actin cables, as assayed both in *myo52+* and *myo52*Δ backgrounds (Figure 3, D and E, and unpublished data). Myo51 tail truncation did not have consequences for the rates of For3-3GFP retrograde flow (Figure 3F; *myo51Δtail-12myc myo52*Δ rate, 0.277 ± 0.113 μm/s, $n = 71$). We note that 3YFP tagging did not impair Myo51 function in actin cable organization (Figure 3E). Thus, in contrast to Myo52, Myo51 decorates actin cables and plays a tail-independent function in actin cable organization.

Possible modes of action of Myo52 on actin cables

We focused on the function of Myo52 and its cargo-binding requirement in cable organization. Thus all further experiments were performed in a *myo51*Δ background to reveal Myo52-specific functions. Two nonexclusive models can be considered (Figure 4). First, Myo52 may deliver a cargo necessary for the regulation of cable assembly at cell tips, for example, promoting formin activity. In this scenario the nature of the cargo and its delivery to cell tips are essential for Myo52 function in cable organization. Second, Myo52 may provide a physical pulling force on the actin cable to extend the actin cable through the cytoplasm. This force may also increase formin polymerization rates, as proposed by previous modeling work (Kozlov and Bershadsky, 2004), resulting in higher rates of actin assembly and retrograde flow. For retrograde force production, Myo52 may be anchored statically at the cell cortex or use a mobile load (like an organelle) that produces a drag due to friction with a viscous cytoplasm. This second model, which is in agreement with the slower actin retrograde flow in *myoV* mutants, predicts that cargo binding, but not the nature of the cargo, and translocation of Myo52 along the cable are necessary for Myo52 function.

A kinesin–myosin chimera improves actin cable organization in *myoV* mutants

To test whether delivery of Myo52 cargoes to tips would be sufficient for actin cable organization independently of translocation along actin cables, we used a kinesin–myosin fusion protein in which the actin-based motor of Myo52 is replaced by the microtubule-based motor of the kinesin-7 Tea2 (Tea2N-GFP-Myo52C; see Figure 5B; Lo Presti and Martin, 2011). This motor chimera is functional, as it restores polarized cell growth and viability to cells lacking actin cables (Lo Presti and Martin, 2011). Phalloidin staining and GFP-CHD_{Rng2} live imaging showed that this chimera attenuates the cable defect of *myoV*Δ cells, decreasing the percentage of cells with misoriented or thick cables (Figure 5, A–D). This partial

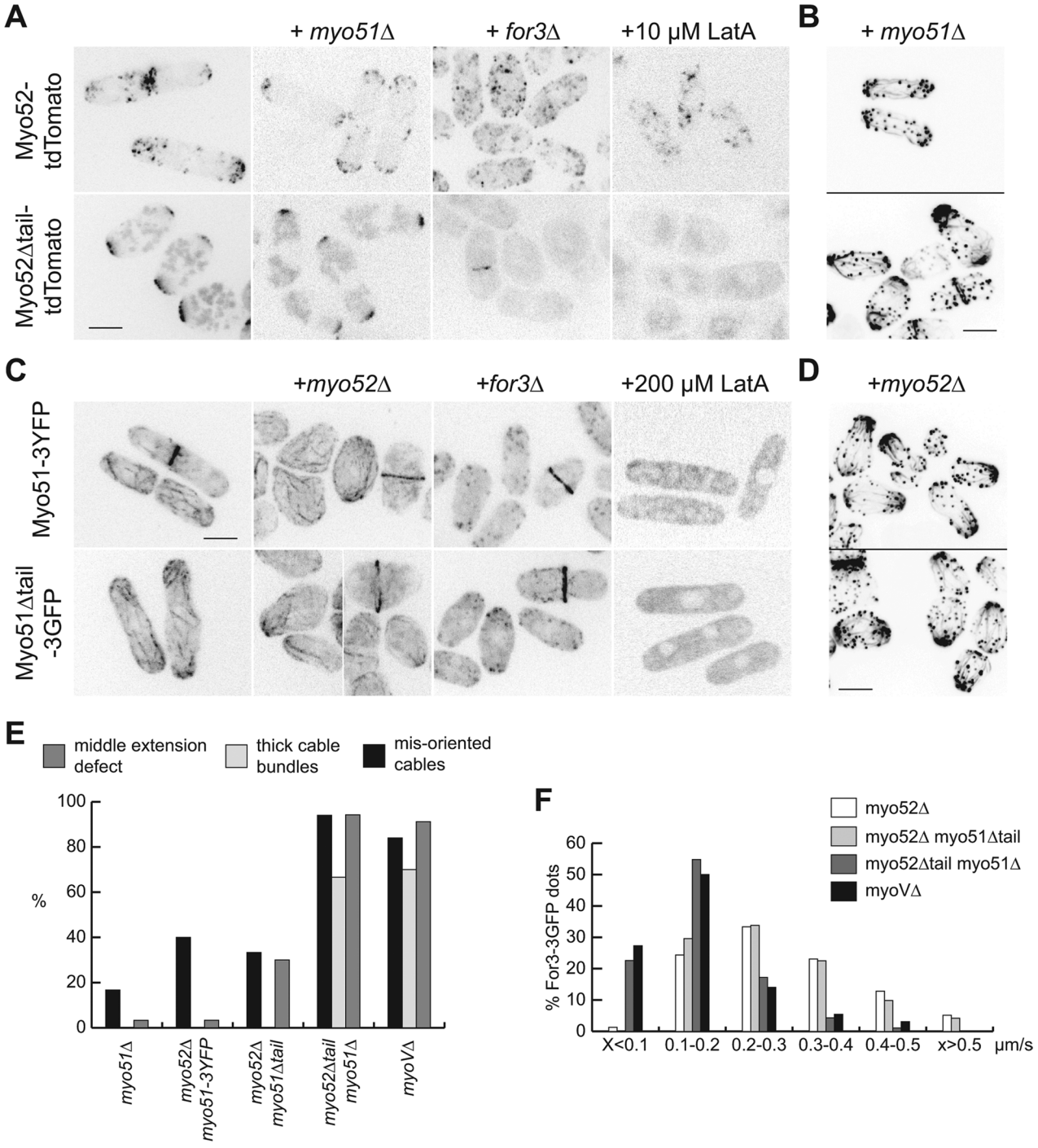

FIGURE 3: Differential requirement of the C-terminal tail for Myo51 and Myo52. (A) Cells expressing either Myo52-tdTomato (top) or Myo52Δtail-tdTomato (bottom) in otherwise wild-type (left), *myo51*Δ, and *myo51*Δ *for3*Δ backgrounds and in wild type after 15-min treatment with 10 μM Lat(A). (B) Alexa Fluor–phalloidin staining of *myo51*Δ cells expressing Myo52-tdTomato (top) or Myo52Δtail-tdTomato (bottom). Inverted images. (C) Cells expressing either Myo51-3YFP (top) or Myo51Δtail-3GFP (bottom) in otherwise wild-type (left), *myo52*Δ, and *for3*Δ backgrounds and in wild type after 5-min treatment with 200 μM Lat(A). (D) Alexa Fluor–phalloidin staining of *myo52*Δ cells expressing Myo51-3YFP (top) or Myo51Δtail-3GFP (bottom). Inverted images. (E) Quantification of the actin defect as assessed in B and D. (F) Histogram distribution of retrograde For3p-3GFP dot rates. The 3GFP in myo51Δtail-3GFP was replaced with a 12myc tag in order to measure For3-3GFP dot rates. Tag replacement had no effect on actin organization as assessed by phalloidin staining (unpublished data). Scale bars, 5 μm.

rescue was dependent on microtubules, as Tea2N-GFP-Myo52C had no effect on actin cables in cells lacking the EB1 homologue Mal3, necessary for microtubule function (Beinhauer *et al.*, 1997). However, the chimera failed to rescue the extension of cables through the cell and the retrograde flow defect (0.155 ± 0.106 μm/s, $n = 166$; Figure 5C and Figure 8C later in the paper).

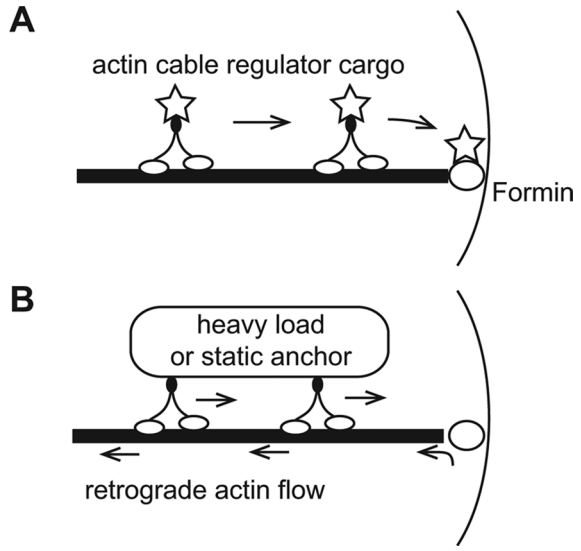

FIGURE 4: Possible mechanisms of cable regulation by Myo52. (A) Myosin V may play a transport function by delivering an actin cable regulator to cell tips. (B) Myosin V may exert a direct physical action on cables by pulling them toward the cell interior while displacing a heavy cargo toward the tips.

These data suggest that cargo delivery is in part sufficient to regulate actin cable organization but not dynamics.

Myo52 associates with For3

What cargo does Myo52 deliver to the tips for actin organization? All known For3 regulators—Bud6, Pob1, Tea4, active Cdc42 as labeled with CRIB-GFP—as well as the CLIP170 protein Tip1, previously shown to bind Myo52, localized correctly to cell tips in *myoV*Δ cells (Supplemental Figure S4; Martin *et al.*, 2005, 2007; Martin and Chang, 2006; Martin-Garcia and Mulvihill, 2009; Rincon *et al.*, 2009), suggesting that none of these is a Myo52 cargo. In wild-type cells, a small subset of For3-3GFP dots exhibit tip-bound (anterograde) movements with an average rate of 1.15 ± 0.68 μm/s (n = 30; see also (Martin and Chang, 2006), similar to the rate we measured for Myo52-GFP movements (1.04 ± 0.32 μm/s, n = 30; Figure 6A and Supplemental Movie S5). In *myoV*Δ cells, we did not detect For3 dot movements at these rates. Furthermore, in *myoV*Δ *tea2N-CFP-myo52C* cells, we observed For3-3GFP dots moving toward the cell tips at the slow rate of 3.3 ± 1.0 μm/min (n = 14; Figure 6B), a rate similar to that measured for Tea2N-CFP-Myo52C dots (Lo Presti and Martin, 2011). Myo52-GFP and For3-myc also coimmunoprecipitated (Figure 6C). Taken together, these results suggest that For3 associates with Myo52 and may be transported by Myo52 to cell tips, either through direct interaction or by hitching a ride on vesicles. This may serve to recycle For3 back to the site of actin cable assembly and may contribute to the altered For3 FRAP dynamics observed in *myoV* mutant cells (Figure 2D). Alternatively, the Myo52–For3 interaction may serve to regulate For3 activity at cell tips.

Tethering of Myo52 motor to the nuclear envelope rescues retrograde flow in *myoV*Δ cells

To test whether tension is per se sufficient to pull actin cables through the cell, we designed a second chimera by linking Myo52 motors to the nucleus as heavy cargo. Such artificial load may uncouple the drag produced by a cargo from the effects that physiological Myo52 cargoes may have on actin organization when they are delivered at the tips. We fused the motor and coiled-coil domains of Myo52 with GFP (or cyan fluorescent protein [CFP]) and Nup146, the fission yeast orthologue of *S. cerevisiae* Nup159, a nucleoporin exclusively localized on the cytoplasmic side of the nuclear pore complex (Stelter *et al.*, 2007; Figure 7A). As control, we

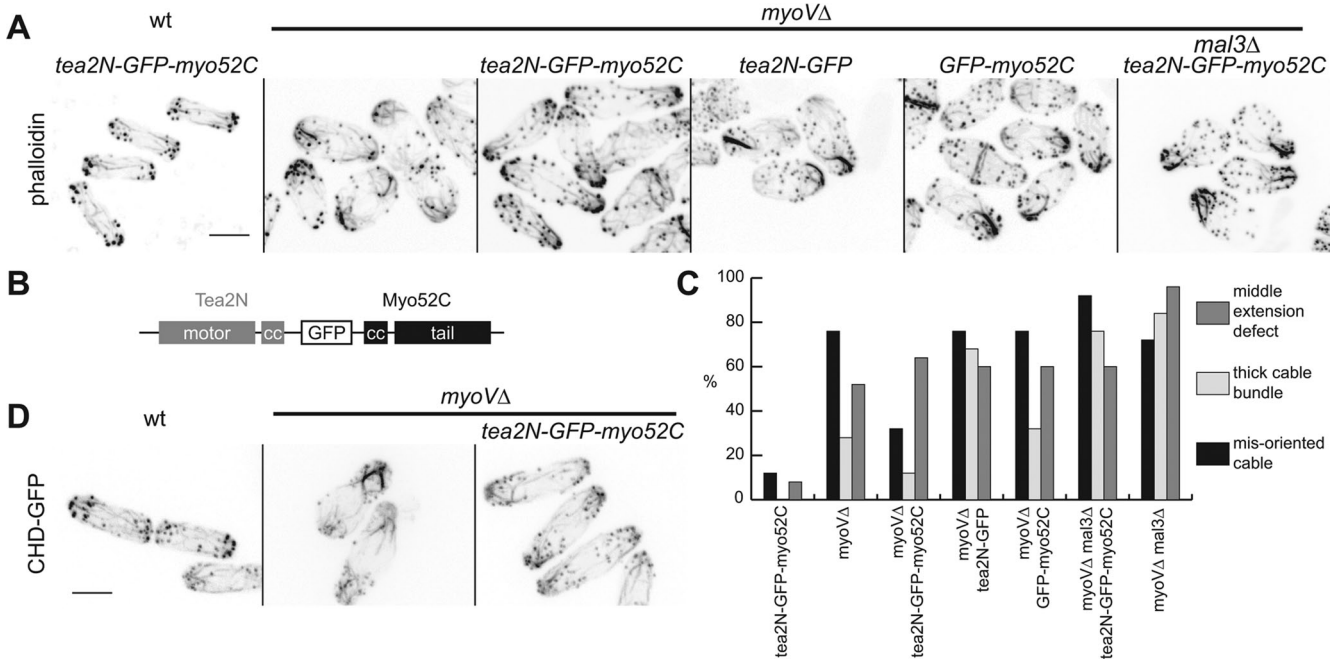

FIGURE 5: A kinesin 7–myosin V chimera attenuates the cable defect of *myoV* null cells. (A) Alexa Fluor–phalloidin staining of wild-type and *myoV*Δ cells expressing Tea2N-GFP-Myo52C and control constructs in *mal3+* and *mal3*Δ backgrounds. (B) Schematic representation of the chimera Tea2N-GFP-Myo52(C). (C) Quantification of the actin defect as assessed in A. (D) Actin organization in live cells expressing the actin marker GFP-CHD_{Rng2}. Inverted images are shown throughout. Scale bars, 5 μm.

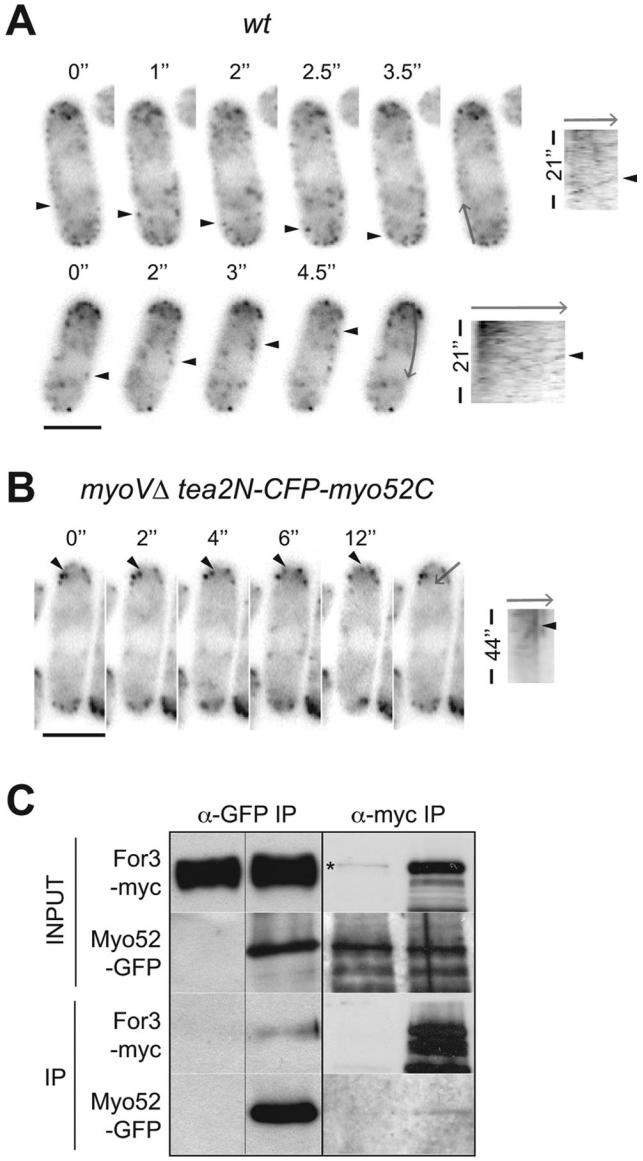

FIGURE 6: Myo52 interacts with For3 and contributes to its delivery to cell tips. (A) Inverted time-lapse images and corresponding kymographs of For3-3GFP anterograde movements in wild-type cells (see Supplemental Movie S5 for other examples). (B) Inverted time-lapse images and corresponding kymographs of For3-3GFP anterograde movements in *myoV*Δ cells expressing the chimera Tea2N-CFP-Myo52(C). Note that replacing GFP with CFP did not alter the localization of the chimera. (C) For3-myc and Myo52-GFP coimmunoprecipitate. Extracts from cells expressing either Myo52-GFP or For3-myc or coexpressing both were immunoprecipitated with anti-GFP (left) or anti-myc antibodies (right) and blotted with anti-GFP and anti-myc antibodies. Samples were loaded either on a 5% (left) or an 8% SDS–PAGE gel (right), which explains the difference in the band patterns between the two experiments. Untagged strains were used as negative controls. The asterisk indicates a background band. Scale bars, 5 μm.

mutated the ATP-binding site of Myo52 motor domain, generating Myo52^{m4A}-CFP-Nup146, a mutant shown to fail to localize to actin structures (Motegi *et al.*, 2001). We also created Myo52N-GFP (or Myo52N-CFP), in which the motor and coiled-coil domains of Myo52 are simply fused with GFP. These constructs were expressed as sole genomic copies in *myoV*Δ cells under the control of the weak *nmt1* promoter. Except for its promoter, Myo52N-GFP is similar to the Myo52Δtail allele described previously (Figure 3A). Fluorescence intensity measurements showed that Myo52N-CFP-Nup146 is expressed at near-endogenous Myo52 levels (1.6-fold up), and Myo52^{m4A}-CFP-Nup146 is modestly (1.9-fold) and Myo52N-CFP is more significantly (2.5-fold) overexpressed (Figure 7B). Myo52N-GFP-Nup146 localized at the nuclear envelope and at tips, reflecting a combination of both endogenous Nup146 and Myo52 localizations (Figure 7C). As expected, Myo52^{m4A}-CFP-Nup146 localized only to the nuclear periphery, whereas Myo52N-GFP, like Myo52Δtail-tdTomato, localized exclusively at cell tips. CFP constructs displayed the same localizations.

The nucleus is normally centered in the cell by a balance of forces exerted by microtubules nucleated from the nuclear periphery and pushing against cell tips (Tran *et al.*, 2001; Tolic-Norrelykke *et al.*, 2005; Daga *et al.*, 2006). The nucleus was centered in most (96%) wild-type cells expressing the Myo52N-GFP-Nup146 chimera. However, upon microtubule depolymerization with MBC for 1h 30 min, the nucleus moved toward one cell pole in 44% of the cells (Figure 7D). Disruption of actin cables with 10 μM LatA prevented this displacement (Figure 7D). Time-lapse imaging of wild-type cells immediately upon MBC treatment demonstrated continuous, slow nuclear movement toward one cell pole in 49% of interphase cells at a rate of 0.065 ± 0.04 μm/min (n = 18; Figure 7F). Thus, in these cells, Myo52 motors are able to transport the whole nucleus along actin cables toward the cell tip.

In *myoV*Δ cells, Myo52N-GFP-Nup146 expression led to nuclear displacement near one cell pole in a large fraction of cells (57%, n = 260), even without MBC addition (Figure 7C). This efficient nuclear displacement by Myo52N-GFP-Nup146 in *myoV*Δ may be partly due to reduced microtubule forces, as microtubules are more numerous but disorganized in this background (Lo Presti and Martin, 2011). As predicted, Ypt3 was delocalized in these cells, as in *myoV*Δ cells (Lo Presti and Martin, 2011), indicating that the Myo52N-GFP-Nup146 chimera does not interact with the normal Myo52 cargoes (Figure 7E). We note that Myo52^{m4A}-CFP-Nup146 and Myo52N-CFP constructs had no effect on nuclear localization (Figure 7C). Thus the nucleus serves as cargo for the myosin–nucleoporin chimera.

Myo52-CFP-Nup146 decreased the percentage of cells with misoriented cables and rescued the cable extension defect of *myoV*Δ cells (Figure 8, A and B). Of importance, this chimera increased retrograde flow rate to an average value of 0.27 ± 0.103 μm/s (n = 67), similar to that of *myo51*Δ and significantly different from that of myoVΔ (t test $p = 2e^{-11}$; Figure 8C). Myo52^{m4A}-CFP-Nup146 had no effect on either cable organization or retrograde flow. GFP-CHD$_{rng2}$ live imaging confirmed these results (Figure 8D). Overexpression of the tail-less Myo52N-CFP also partly ameliorated cable extension and slightly increased retrograde flow rate to an average value of 0.214 ± 0.09 μm/s (n = 48). In contrast, Myo52Δtail expressed at lower levels did not improve cable organization or dynamics (see Figures 3 and Supplemental Figure S2C). Thus increasing either the load of individual motors or the number of motors traveling along cables promotes retrograde flow and actin cable extension through the cell, with load increase being more efficient. These data show that direct pulling forces by Myo52 motors are sufficient to orient cables and increase retrograde flow in vivo.

DISCUSSION

The organization and distribution of actin filaments are central to the cell's general architecture. In particular, efficient vectorial transport of cargoes by myosin motors likely depends not only on the polarity but also on the distribution of tracks through the cell. Here we

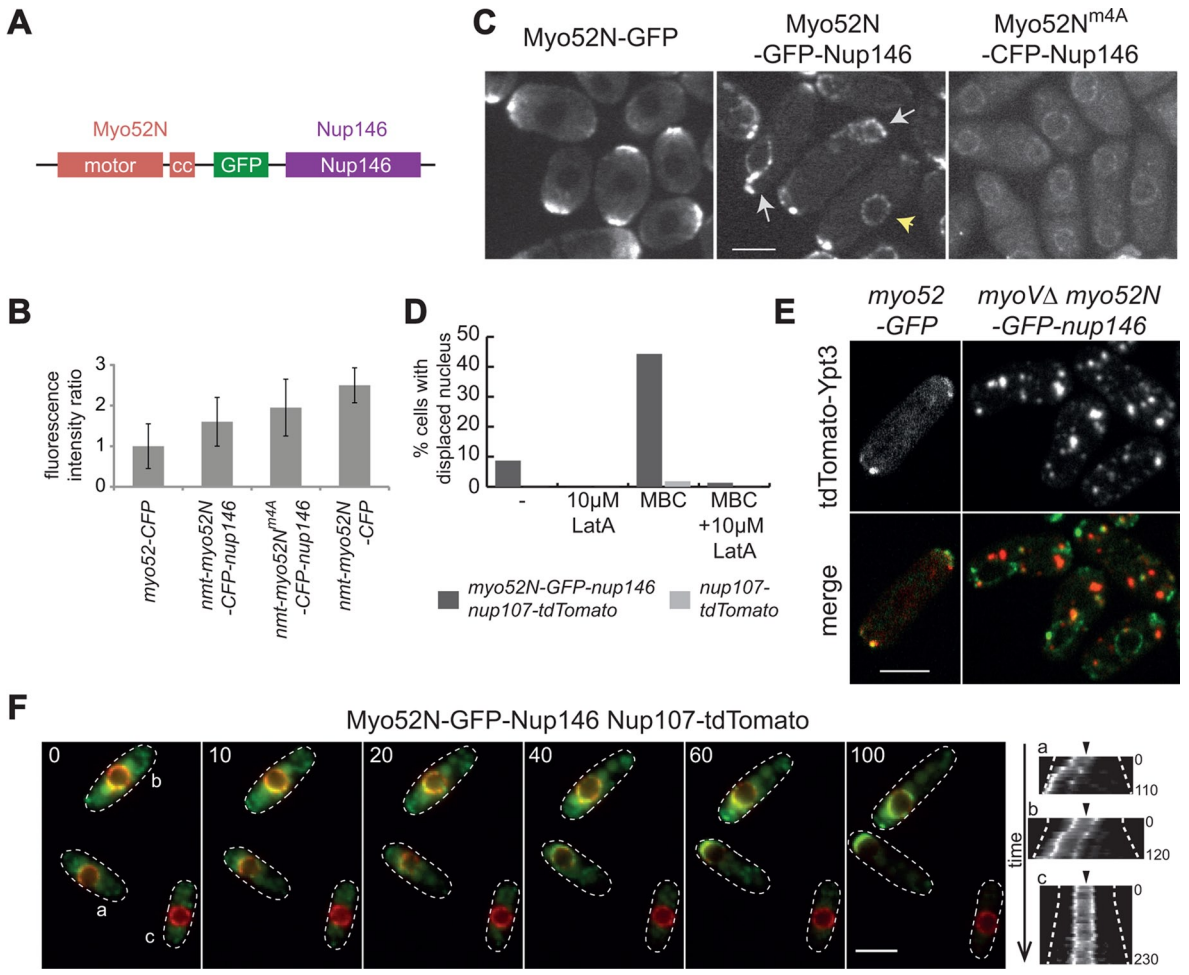

FIGURE 7: Nucleus-tethered Myo52 motors translocate the nucleus along actin cables. (A) Schematic representation of the chimeric protein Myo52N-GFP-Nup146. (B) Quantification of fluorescence intensities of Myo52N-CFP-Nup146, Myo52^{m4A}-CFP-Nup146 and Myo52N-CFP expressed under the control of the weak *nmt1* promoter in *myoV*Δ cells relative to endogenously expressed full-length Myo52-CFP. Error bars, SD. (C) Localization of Myo52N-GFP-Nup146 and control constructs in *myoV*Δ cells. White arrows point to displaced nuclei near the cell tip. The yellow arrow points to a centrally placed nucleus. (D) Effects of 10 μM LatA and 25 μg/ml MBC on nuclear displacement by the chimera Myo52N-GFP-Nup146 in wild-type cells coexpressing the nuclear envelope marker Nup107-tdTomato. Cells were treated for 90 min with the indicated drugs before imaging. E tdTomato-Ypt3 localization in wild-type cells coexpressing Myo52-GFP and *myoV*Δ cells coexpressing Myo52N-GFP-Nup146. (F) Time-lapse images of wild type cells coexpressing Myo52N-GFP-Nup146 and Nup107-tdTomato together with wild-type cells expressing only Nup107-tdTomato. Cells were imaged immediately upon placement on a 2% agarose pad containing MBC at a final concentration of 25 μg/ml. Kymographs of a 2-pixel-wide line across the length of labeled cell are shown on the right. Arrowheads mark the cell middle. Dotted lines outline the edges of the cells. Scale bars, 5 μm.

describe how myosin V not only transports cargoes to cell poles in fission yeast but also organizes its own actin cable tracks. In the absence of myosin V, actin cables are less dynamic, fail to extend through the cell, and are often curled and bundled near cell poles. Through synthetic approaches we experimentally demonstrate two possible distinct contributions of myosin V to cable organization in vivo: through transport of actin regulators to cell poles and through force generation to pull the cables. Taken together, these results suggest that myosin V and actin cables form a self-organizing system in which myosin V shapes the tracks it uses for transport.

Actin cable organization through displacement and delivery of cargoes

The cargo-binding tail of Myo52 is essential for its role in actin cable organization. Using a synthetic biology approach, we artificially separated two distinct elements of cargo transport— delivery of the cargo to the site of action and movement of cargo-bound myosins—and demonstrated that both contribute to cable organization. First, a kinesin–myosin chimera, which delivers myosin cargoes to cell tips using the microtubule network without using the actin tracks and restores polarized cell growth (Lo Presti and Martin, 2011), ameliorates actin cable organization. Second, linking an artificial high load—the nucleus—to the myosin motor traveling along actin cables also partly restores cable organization. These data suggest that both the nature of the transported cargo and the transport action per se contribute to the distribution of actin cables in the cell. These two elements have distinct effects. Although delivery of cargoes to cell tips with the kinesin–myosin chimera improves cable bundling and orientation, this does not influence retrograde flow or cable extension through the cell. In contrast, high load increases

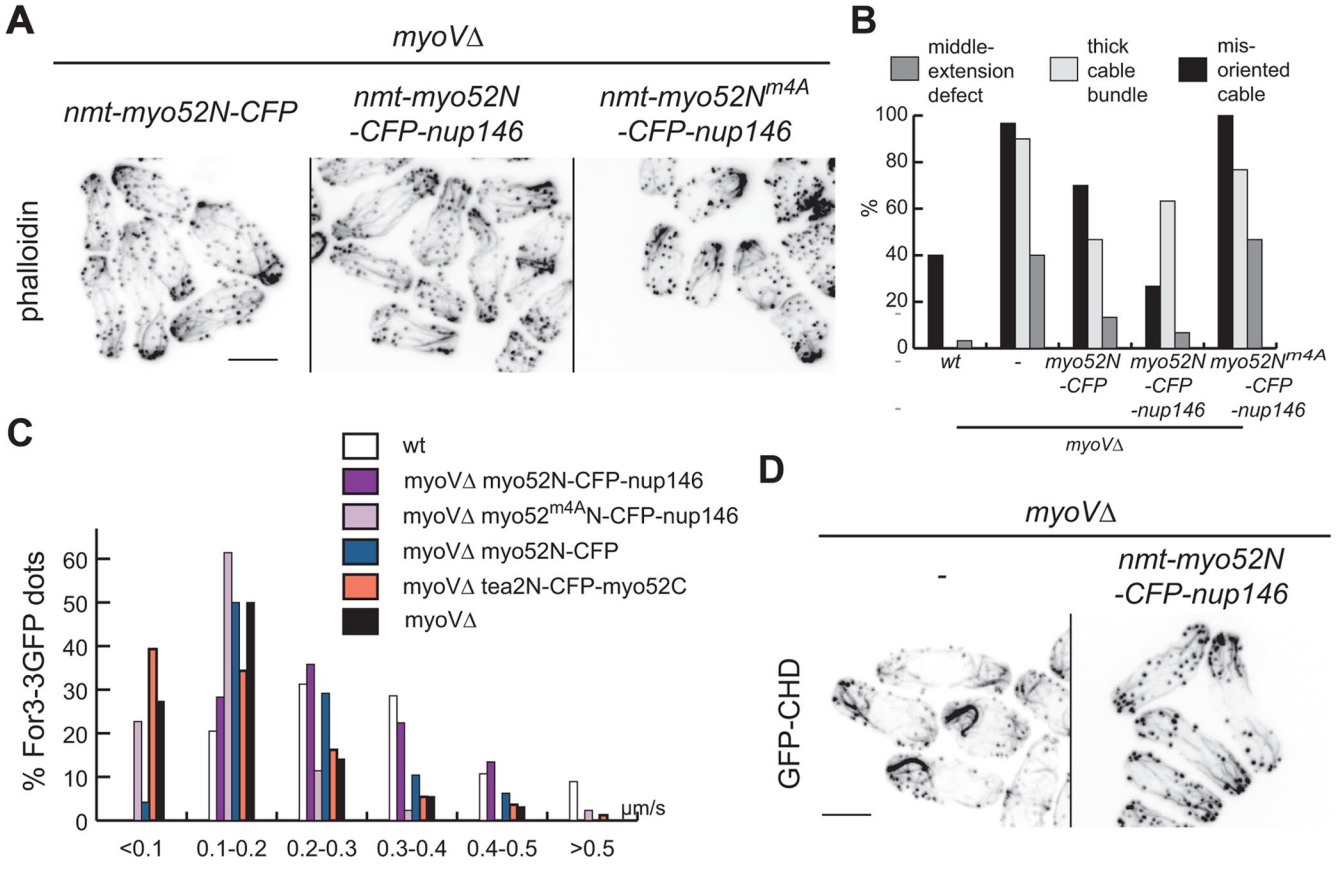

FIGURE 8: Tethering the motor domain of Myo52 to the nucleus increases retrograde flow and cable extension. (A) Alexa Fluor–phalloidin staining in cells expressing the corresponding CFP-labeled constructs. Note that replacing GFP with a CFP tag altered neither the localization of the chimera nor that of the control constructs. (B) Quantification of the actin defect as assessed by phalloidin staining in A. (C) Histogram distribution of retrograde For3p-3GFP dot rates in indicated strains. See text for details. (D) Live-cell imaging of GFP-CHD_{Rng2} in *myoV*Δ cells in the absence or upon the expression of the chimera Myo52N-GFP-Nup146. Inverted images are shown throughout. Scale bars, 5 μm.

retrograde flow, cable extension, and orientation but not bundling. Thus delivery and transport movement may contribute complementary functions for actin cable organization.

Role of tension in actin cable dynamics

Myosin Vs contribute to actin cable orientation along the length of the cell. By applying an artificial load to Myo52, we show that tension is sufficient to straighten the cables. By walking on the cable, Myo52 may pull on the cable. Because the cables are anchored by the formin For3 at cell poles and are significantly longer than the width of the cell, this promotes straightening of the cable along the cell length.

Myosin Vs also contribute to the retrograde flow of cables, which again may be due to load-dependent force generation on the cable. The retrograde flow of actin is powered by actin polymerization, which, in the case of actin cables, is driven by formins (Martin and Chang, 2006; Buttery *et al.*, 2007). For actin cables to remain anchored at the cell tips, the rates of actin assembly and retrograde flow must be coordinated. Our data thus suggest that Myo52-induced cable tension increases the rate of actin polymerization and thus For3 activity. This idea is also supported by previous modeling work that suggests that a pulling force on actin filaments would enhance formin-based actin polymerization (Kozlov and Bershadsky, 2004). Myo52 may thus promote retrograde flow by directly pulling on the cable and enhancing formin-driven polymerization at cell poles.

Myo52 pulling forces likely encounter significant resistance in cables: whereas we measured Myo52 anterograde movements in the 1-μm/s range, the combined action of both Myo51 and Myo52 leads to increase in retrograde flow by only ~0.15 μm/s. This is distinct from the 2-μm/s actin cable translocation rate observed in unpolarized *S. cerevisiae* cells (Yu *et al.*, 2011). This modest increase in retrograde flow may be constrained by the maximal polymerization rate of the formin For3 (Scott *et al.*, 2011), which anchors the cables at the cell pole. Alternatively, it may come about not from an immobilized motor at the cell periphery but from the resistance encountered when moving cargoes, which converts only part of the relative displacement into cable movement. This is the case when the nucleus is used as artificial load or upon overexpression of the tail-less Myo52. Note that this truncated Myo52 allele may retain residual cargo interactions, as recent evidence in *S. cerevisiae* showed that some of the interactions with exocytic vesicles occur through the myosin V coiled-coil region (Robinson *et al.*, 1999; Gangar *et al.*, 2005; Rossi and Brennwald, 2011)

Although the nucleus is unlikely to be the relevant physiological load, myosin V motors have been described to transport a range of other organelles. Interaction and transport of the endoplasmic reticulum (ER), vacuoles, peroxisomes, and exocytic vesicles have been documented in *S. cerevisiae* (Hammer and Sellers, 2012). Beyond yeast, myosin V also transports ER tubules into dendritic spines (Wagner *et al.*, 2011), and myosin XI, which structurally and

functionally replaces class V in plants, drives ER motility (Ueda *et al.*, 2010). In *Schizosaccharomyces pombe*, Myo52 binds exocytic vesicles through Ypt3 (Lo Presti and Martin, 2011). It may also interact with vacuoles through Ypt3, as *myo52Δ* and *ypt3-i5* cells are defective in vacuole fusion (Mulvihill *et al.*, 2001; Cheng *et al.*, 2002). However, there is no evidence for vacuoles as Myo52 cargoes. The ER may also be a cargo for MyoV: we observed that, in contrast to wild-type cells, in which the ER covers the entire nuclear and cell periphery, *myoVΔ* cells display large ER gaps at the poles and septa (Lo Presti and Martin, unpublished data). Either or all of these organelles may serve as load for actin cable extension through the cell.

Myosin V Myo52 may deliver cable organizers to cell poles

Partial cable rescue by the kinesin–myosin chimera suggests that Myo52 also promotes actin cable organization through delivery of actin assembly factors to cell tips. We suggest that For3 may be a novel cargo for Myo52: For3 and Myo52 coimmunoprecipitate, and For3 movement toward cell tips occurs at the same rate as that of Myo52 tail, whether it is linked to the endogenous myosin motor or to Tea2 kinesin motor. We note, however, that the number and run lengths of movements observed with the Tea2 chimera are low, probably in part due to the necessity to image For3-3GFP through the YFP channel to avoid bleedthrough signal from the CFP-tagged chimera. Although Myo52 or actin cables are not required for For3 association with cell tips (Martin and Chang, 2006), Myo52-driven delivery of For3 to cell poles may compensate for For3 loss by retrograde flow, forming a feedback mechanism conferring balance to a dynamic system. Alternatively, Myo52 association with For3 may serve to regulate the formin activity or promote its release from the cell tip, and the For3 anterograde movements observed may in fact represent a by-product of an association that normally occurs at cell tips.

Indeed, how For3 delivery to poles may then control bundling and orientation of cables is not immediately evident, as at least in vitro For3 lacks bundling activity (Scott *et al.*, 2011). This suggests that Myo52 delivers at cell poles additional cargo (cargoes) that modulate cable organization. In budding yeast, for instance, the myosin V Myo2 has been recently shown to deliver to the sites of F-actin assembly a distant member of the kinesin 1 family, Smy1, which dampens the activity of the formin Bnr1 (Chesarone-Cataldo *et al.*, 2011). The kinesin–myosin chimera efficiently transports Ypt3-linked vesicles to cell poles, in addition to For3, and thus restores polarized secretion (Lo Presti and Martin, 2011). In turn, actin patches (and thus endocytosis) are repolarized to cell poles (Gachet and Hyams, 2005). This may even have indirect consequences on actin cable organization. For instance, For3 clusters at the plasma membrane may be more easily dispersed upon increased membrane trafficking, thus decreasing the chance of cable bundle formation. By restoring the processes of exocytosis and endocytosis, the kinesin–myosin chimera may also restore normal levels of plasma membrane phosphoinositide species known to regulate ABPs (Saarikangas *et al.*, 2010).

Roles of myosin V Myo51 and microtubules in actin cable organization

The second myosin V, Myo51, also contributes to actin cable organization, but likely through a distinct mechanism. First, Myo51 tail truncation does not perturb actin cables, suggesting that Myo51's function in cable organization may be cargo independent. We note, however, that the coiled-coil domain of some myosin Vs also has roles in cargo binding (Robinson *et al.*, 1999; Gangar *et al.*, 2005; Rossi and Brennwald, 2011), suggesting that Myo51 may still bind partners for cable organization. Second, Myo51 decorates the length of actin cables and localizes to actin patches in the absence of cables. Preferential cable binding may be conferred by tropomyosin, which stabilizes actin cables and enhances Myo51 actin binding in vitro (Balasubramanian *et al.*, 1992; Clayton *et al.*, 2010). A key question for the future is whether Myo51 plays a novel structural role in regulating actin assemblies.

In the absence of both Myo51 and Myo52, microtubules may contribute to actin cable organization, since microtubule disruption exacerbates the cable defect of *myoVΔ* cells. Interactions between the actin and microtubule cytoskeletons are well documented and underlie many fundamental processes, such as morphogenesis, cell motility, and division (Rodriguez *et al.*, 2003). In fission yeast a regulatory interaction between microtubules and actin is proposed to control the transition from monopolar to bipolar growth (Martin *et al.*, 2005). Whether microtubules exert a regulatory function or physically interact with actin cables to promote their extension through the cell in absence of type V myosin is unknown but deserves further investigation.

Myosin V and actin: a self-organizing system

Transport myosins may organize actin tracks in other organisms. Myosin V influences actin cable dynamics in *S. cerevisiae* (Yu *et al.*, 2011), driving the cortical translocation of cables in unpolarized cells. However, it plays no or only a modest role in the organization of polarized cables, in which bud neck–localized type II myosin contributes to the retrograde flow of these cables by pulling them through the neck (Huckaba *et al.*, 2006). Budding yeast cells may have developed an ad hoc mechanism to overcome the impediment imposed by the bud neck, masking the possible contribution of myosin V in cable organization. In the moss *Physcomitrella patens* and in *Arabidopsis thaliana*, loss of the transport motor, myosin XI, also alters F-actin organization (Peremyslov *et al.*, 2010; Vidali *et al.*, 2010) and ER motility (Ueda *et al.*, 2010), suggesting that ER-loaded myosin also contributes in these cells to shape its own tracks.

Collectively our data reveal elements of a self-organizing system in which myosin Vs do not passively use actin filaments but actively shape their own tracks: cargo transport promotes the extension of the tracks that allowed cargo transport in the first place. By promoting a better distribution of cables through the cell space, myosin V ensures that any cellular region finds itself in relatively close average proximity to actin cables, favoring cargo–motor–track interaction and cargo transport.

MATERIALS AND METHODS

Strains, growth conditions, and pharmacological inhibitor

Standard genetic methods and growth conditions were used. Cells were grown in Edinburgh minimal media (EMM) supplemented with appropriate amino acids (ALU) or YE5S as indicated. Particular care was taken to avoid accumulation of suppressors in poorly growing strains by backcrossing, by rapid stocking of newly generated strains, and by streaking them freshly at each experiment.

S. pombe strains used in this study are listed in Supplemental Table S1. Tagged and truncation strains were constructed by using either a PCR or an integrative plasmid–based approach (Bahler *et al.*, 1998; Martin and Chang, 2006) and confirmed by PCR. The *myo51Δtail-3GFP* (or -12myc) strain produces a Myo51 product truncated at amino acid 1087. The *myo52Δtail-tdTomato* strain produces a Myo52 product truncated at amino acid 1162.

MBC (Sigma-Aldrich, St. Louis, MO) was used at final concentration of 25 μg/ml from a stock of 2.5 mg/ml in dimethyl sulfoxide

(DMSO). MBC treatment was performed for 30 min at 30°C unless otherwise indicated.

Latrunculin A (Phillip Crews, University of California, Santa Cruz, Santa Cruz, CA) was used at final concentration of 10 or 200 µM as indicated from a stock of 20 mM in DMSO. LatA treatment was performed for 15 min either at 25° or 30°C unless otherwise indicated. Control experiments with DMSO had no effect on F-actin organization or fluorescent fusion protein localization.

Molecular biology methods

All plasmids were constructed using standard molecular biology techniques. In general, genes or gene fragments were cloned after PCR using as template genomic DNA or plasmids and primers containing 5′ extensions with specific restriction sites. Details of the primers and restriction sites used are available upon request.

Details about Tea2N-GFP-Myo52C and control constructs can be found in Lo Presti and Martin (2011). The chimera Myo52N-GFP-Nup146 was cloned under control of the weak *nmt* promoter in pRIP82 vector and encodes, in this order, amino acids 1–1162 of Myo52, a SGRA linker, GFP, a GSSGP linker, and full-length Nup146 (UniProtKB accession number Q09847). For the construction of the control chimera Myo52^{m4A}N-GFP-Nup146, pRep81-myo4^{m4A}-YFP was used as template for the amplification of *myo52N* (Motegi *et al.*, 2001). The cassette *myo52N-GFP-nup146* and the control cassettes were linearized and integrated into the *ura4* genomic locus.

Microscopy

Microscopy was performed with either a spinning-disk confocal microscope or a wide-field fluorescence microscope.

For3-3GFP and Myo52N-GFP-Nup146 imaging was mainly performed using a DeltaVision system (Applied Precision, Issaquah, WA) composed of a customized Olympus IX-71 Inverted Microscope Stand (Olympus, Tokyo, Japan) fitted with a PlanApo 100× oil, 1.42 numerical aperture (NA) objective, a CoolSNAP HQ2 camera (Photometrics, Tucson, AZ), and an Insight SSI 7 Color Combined Unit Illuminator. Images were acquired with softWoRx software (Applied Precision, a GE Healthcare Company), using the fast acquisition mode.

FRAP experiments were performed on a laser scanning confocal microscope (LSM510 Meta; Carl Zeiss, Jena, Germany). Photobleaching was obtained by 25 iterative scans of a selected region encompassing the very tip of a cell at maximal laser power. Images were recorded before photobleaching, immediately after, and subsequently every 2 s, with 5% laser power, as described (Martin and Chang, 2006).

All other images were acquired on a spinning-disk system, using a Leica DMI4000B inverted microscope (Leica, Wetzlar, Germany) equipped with an HCX PL APO ×100/1.46 NA oil objective and a PerkinElmer UltraView Confocal system (including a Yokagawa CSU22 real-time confocal scanning head, an argon/krypton laser, and a cooled 14-bit frame transfer electron-multiplying charge-coupled device C9100-50 camera; PerkinElmer, Waltham, MA). Stacks of *z*-series confocal sections were acquired at 0.3-µm intervals with the UltraView or Volocity software (PerkinElmer), and images were rendered by two-dimensional maximum-intensity projection unless otherwise indicated.

Actin staining was performed as described using Alexa Fluor 488–phalloidin (Invitrogen, Carlsbad, CA) with a fixation time of 40–60 min (Bendezu and Martin, 2011). Phalloidin staining was generally performed on cells grown at 30°C in YES5 (yeast extract medium + 5 supplements: 225 mg/l adenine, histidine, leucine, uracil, and lysine hydrochloride), except for strains expressing chimeras, for which cells were grown for 16–24 h at 30°C in EMM-AL to induce expression. For actin staining of GFP-tagged strains, Alexa Fluor 488–phalloidin was also used because the GFP signal was not resistant to the fixation and staining procedure, and thus it did not interfere with imaging of the actin cytoskeleton.

To image live actin cables, we induced GFP-CHD$_{Rng2}$ expression for 16 h in EMM-AU at 30°C, unless otherwise specified. For imaging actin cable dynamics, we acquired a stack of 14 *z*-series confocal sections at 0.3-µm intervals for 90 s with a rate of 0.4–0.8 s per time point. To image chimeric proteins, we induced expression for 24 h in EMM-AL at 30°C. To image both live chimeric proteins and GFP-CHD$_{Rng2}$, expression was induced for 18 h in EMM-AU at 30°C unless otherwise specified.

Image data analysis

For fluorescence intensity measurements, we measured the average fluorescence intensity of sum projections of spinning-disk confocal *z*-stacks of at least five individual cells for each genotype. Background correction was performed by subtracting the background fluorescence intensity in a region that did not contain cells and the autofluorescence levels of wild-type cells expressing no fluorescent marker imaged and processed in the same conditions. All values were normalized to that of endogenous full-length Myo52-tdTomato or Myo52-CFP.

For quantification of the actin defect, we analyzed two-dimensional maximum-intensity projections of phalloidin-stained cells. For each cell, we visually scored the presence of 1) at least one cable oriented in a direction distinct from the longitudinal axis of cell (misoriented cable) and 2) a thick cable bundle. Note that cells bearing thick cable bundles usually had a single thick bundle rather than multiple ones. To count the number of cables extending beyond the cell middle, we used the ObjectJ tool in the ImageJ software (National Institutes of Health, Bethesda, MD) to measure cell length and precisely locate the cell middle. Cells with fewer than three cables crossing this location were assigned a middle extension defect. For each genotype the percentage of cells displaying any of the three parameters was calculated and plotted. Up to 16 independent experiments for a total of 480 cells were quantified, with 25–30 cells assessed each time. The graphs show data from one of them. Phalloidin staining quality varies from one experiment to the next. In particular, growth of the cells in rich (YE5S) or minimal (EMM) medium has significant impact on the quality of the staining, with actin cables consistently better detected for cells grown in rich medium. Therefore, each graph represents one set of stainings conducted in parallel, and numbers across experiments cannot be directly compared. However, the trends shown in the graphs are the same in all repeats. The precise number of independent experiments/total number of cells quantified are as follows: wild-type, 9/270; myo51Δ, 7/210; myo52Δ, 2/60; myoVΔ, 16/480; myoVΔ tea2N-myo52C, 6/180; myoVΔ tea2N, 2/60; myoVΔ myo52C, 2/60; myoVΔ mal3Δ tea2N-myo52C, 1/30; myoVΔ myo52N-nup146, 4/120; myovΔ myo52N, 3/90; myoVΔ myo52N^{m4A}-nup146, 2/60; myo51Δtail myo52Δ, 2/60; myo52Δtail myo51Δ, 2/60; myoVΔ cdc25-22, 1/27; myo51Δ cdc25-22, 1/27; mal3Δ, 3/90; and mal3Δ myoVΔ, 4/120.

For analysis of the FRAP experiments, the mean fluorescence intensities were measured over time in three regions: 1) the photobleached region, 2) the background, and 3) another nonbleached cell. For each time point, the intensities of the bleached region and of the unrelated cell were adjusted by subtracting background signal. To correct for loss of signal due to imaging, the adjusted bleached region intensity was then divided by the adjusted intensity of the other cell. For each experiment, all values were normalized so

that the photobleached value equals 0 and the prephotobleaching value equals 1. Finally, averages and standard errors were derived for fluorescence values at individual time points.

For3-3GFP dots and nuclear displacement rates were quantified using the softWoRx tool Leap Frog and averaged using Excel (Microsoft, Redmond, WA). Quantification of nuclear translocation in cells expressing Myo52N-GFP-Nup146 was done on images acquired at the DeltaVision using the ImageJ plug-in Cell Counter to count the number of interphase cells with a nucleus at the very cell end versus the total number of interphase cells. Figures were prepared with Photoshop Elements 6 and Illustrator CS3 (Adobe, San Jose, CA), and movies were prepared using ImageJ 1.41.

Biochemical methods

Extracts from yeast grown in EMM-AU medium for 21 h at 30°C were prepared in CXS buffer (50 mM 4-(2-hydroxyethyl)-1-piperazineethanesulfonic acid, pH 7.0, 20 mM KCl, 1 mM $MgCl_2$, 2 mM EDTA, pH 7.5, and protease inhibitor cocktail) by grinding in liquid nitrogen with a mortar and pestle. After thawing, NaCl and Triton X-100 were added to final concentrations of 150 mM and 0.1%, respectively. For immunoprecipitations, 150 µl of soluble extract was added to 20 µl of sheep anti-mouse magnetic Dynabead slurry (Dynal, Invitrogen) prebound to 2 µg of monoclonal anti-Myc antibodies (9E10; Santa Cruz Biotechnology, Santa Cruz, CA) and incubated for 2 h at 4°C. Magnetic Dynabeads were then washed four times in CXS and 0.1% Triton and three times in IPP150 (150 mM Tris, pH 8.0, 150 mM NaCl, 0.1% Nonidet P40, 2 mM EDTA, 1 mM $MgCl_2$). Immunoprecipitated material was then recovered by boiling Dynabeads in 60 µl of SDS sample buffer for 5 min at 95°C. Standard protocols were used for SDS–PAGE and Western blot analysis. Antibodies used for immunoprecipitations and Western blots were mouse monoclonal anti-Myc (9E10; Santa Cruz Biotechnology), mouse monoclonal anti-GFP (Roche, Indianapolis, IN), and rabbit polyclonal serum anti-GFP (A6455; Invitrogen).

ACKNOWLEDGMENTS

We thank T. Kuno (Kobe University School of Medicine, Kobe, Japan), P. Perez (University of Salamanca, Salamanca, Spain), M. Lord (University of Vermont, Burlington, VT), and I. Mabuchi (University of Tokyo, Tokyo, Japan) for strains and/or plasmids. We thank present and former members of the Martin laboratory, in particular Felipe Bendezu, for critical discussion. This work was supported by Swiss National Science Foundation Professorship Grant PP00A-114936 and Research Grant 31003A_138177. Research in the Martin lab is also supported by a Human Frontier Science Program Career Development Award (CDA0016/2008) and a European Research Council Starting Grant (260493). F.C. is supported by National Institute of Health Grants R01 GM0669670 and GM05636.

REFERENCES

Bahler J, Wu JQ, Longtine MS, Shah NG, McKenzie A, Steever AB, Wach A, Philippsen P, Pringle JR (1998). Heterologous modules for efficient and versatile PCR-based gene targeting in *Schizosaccharomyces pombe*. Yeast 14, 943–951.

Balasubramanian MK, Helfman DM, Hemmingsen SM (1992). A new tropomyosin essential for cytokinesis in the fission yeast *S. pombe*. Nature 360, 84–87.

Beinhauer JD, Hagan IM, Hegemann JH, Fleig U (1997). Mal3, the fission yeast homologue of the human APC-interacting protein EB-1 is required for microtubule integrity and the maintenance of cell form. J Cell Biol 139, 717–728.

Bendezu FO, Martin SG (2011). Actin cables and the exocyst form two independent morphogenesis pathways in the fission yeast. Mol Biol Cell 22, 44–53.

Berg JS, Cheney RE (2002). Myosin-X is an unconventional myosin that undergoes intrafilopodial motility. Nat Cell Biol 4, 246–250.

Bohil AB, Robertson BW, Cheney RE (2006). Myosin-X is a molecular motor that functions in filopodia formation. Proc Natl Acad Sci USA 103, 12411–12416.

Brennwald P, Rossi G (2007). Spatial regulation of exocytosis and cell polarity: yeast as a model for animal cells. FEBS Lett 581, 2119–2124.

Buttery SM, Yoshida S, Pellman D (2007). Yeast formins Bni1 and Bnr1 utilize different modes of cortical interaction during the assembly of actin cables. Mol Biol Cell 18, 1826–1838.

Cheng H, Sugiura R, Wu WL, Fujita M, Lu YB, Sio SO, Kawai R, Takegawa K, Shuntoh H, Kuno T (2002). Role of the rab GTP-binding protein Ypt3 in the fission yeast exocytic pathway and its connection to calcineurin function. Mol Biol Cell 13, 2963–2976.

Chesarone MA, DuPage AG, Goode BL (2011). Unleashing formins to remodel the actin and microtubule cytoskeletons. Nat Rev Mol Cell Biol 11, 62–74.

Chesarone-Cataldo M, Guerin C, Yu JH, Wedlich-Soldner R, Blanchoin L, Goode BL (2011). The myosin passenger protein Smy1 controls actin cable structure and dynamics by acting as a formin damper. Dev Cell 21, 217–230.

Clayton JE, Sammons MR, Stark BC, Hodges AR, Lord M (2010). Differential regulation of unconventional fission yeast myosins via the actin track. Curr Biol 20, 1423–1431.

Daga RR, Yonetani A, Chang F (2006). Asymmetric microtubule pushing forces in nuclear centering. Curr Biol 16, 1544–1550.

Doyle A, Martin-Garcia R, Coulton AT, Bagley S, Mulvihill DP (2009). Fission yeast Myo51 is a meiotic spindle pole body component with discrete roles during cell fusion and spore formation. J Cell Sci 122, 4330–4340.

Eppinga RD, Peng IF, Lin JLC, Wu CF, Lin JJC (2008). Opposite effects of overexpressed myosin Va or heavy meromyosin Va on vesicle distribution, cytoskeleton organization, and cell motility in nonmuscle cells. Cell Motil Cytoskeleton 65, 197–215.

Feierbach B, Chang F (2001). Identification of for3, a *S. pombe* formin-homology gene involved in cell polarity, actin cable formation, and symmetric cell division. Mol Biol Cell 12, 49A.

Gachet Y, Hyams JS (2005). Endocytosis in fission yeast is spatially associated with the actin cytoskeleton during polarised cell growth and cytokinesis. J Cell Sci 118, 4231–4242.

Gangar A, Rossi G, Andreeva A, Hales R, Brennwald P (2005). Structurally conserved interaction of Lgl family with SNAREs is critical to their cellular function. Curr Biol 15, 1136–1142.

Grallert A, Martin-Garcia R, Bagley S, Mulvihill DP (2007). In vivo movement of the type V myosin Myo52 requires dimerisation but is independent of the neck domain. J Cell Sci 120, 4093–4098.

Hammer JA, Sellers JR (2012). Walking to work: roles for class V myosins as cargo transporters. Nat Rev Mol Cell Biol 13, 13–26.

He Y, Sugiura R, Ma Y, Kita A, Deng L, Takegawa K, Matsuoka K, Shuntoh H, Kuno T (2006). Genetic and functional interaction between Ryh1 and Ypt3: two Rab GTPases that function in *S. pombe* secretory pathway. Genes Cells 11, 207–221.

Huckaba TM, Lipkin T, Pon LA (2006). Roles of type II myosin and a tropomyosin isoform in retrograde actin flow in budding yeast. J Cell Biol 175, 957–969.

Kamasaki T, Arai R, Osumi M, Mabuchi I (2005). Directionality of F-actin cables changes during the fission yeast cell cycle. Nat Cell Biol 7, 916–917.

Karagiannis J, Bimbo A, Rajagopalan S, Liu JH, Balasubramanian MK (2005). The nuclear kinase Lsk1p positively regulates the septation initiation network and promotes the successful completion of cytokinesis in response to perturbation of the actomyosin ring in *Schizosaccharomyces pombe*. Mol Biol Cell 16, 358–371.

Kozlov MM, Bershadsky AD (2004). Processive capping by formin suggests a force-driven mechanism of actin polymerization. J Cell Biol 167, 1011–1017.

Li JF, Nebenfuhr A (2008). The tail that wags the dog: the globular tail domain defines the function of myosin V/XI. Traffic 9, 290–298.

Lipatova Z, Tokarev AA, Jin Y, Mulholland J, Weisman LS, Segev N (2008). Direct interaction between a myosin V motor and the Rab GTPases Ypt31/32 is required for polarized secretion. Mol Biol Cell 19, 4177–4187.

Lo Presti L, Martin SG (2011). Shaping fission yeast cells by rerouting actin-based transport on microtubules. Curr Biol 21, 2064–2069.

Martin SG, Chang F (2006). Dynamics of the formin For3p in actin cable assembly. Curr Biol 16, 1161–1170.

Martin SG, McDonald WH, Yates JR, Chang F (2005). Tea4p links microtubule plus ends with the formin For3p in the establishment of cell polarity. Dev Cell 8, 479–491.
Martin SG, Rincon SA, Basu R, Perez P, Chang F (2007). Regulation of the formin for3p by cdc42p and bud6p. Mol Biol Cell 18, 4155–4167.
Martin-Garcia R, Mulvihill DP (2009). Myosin V spatially regulates microtubule dynamics and promotes the ubiquitin-dependent degradation of the fission yeast CLIP-170 homologue, Tip1. J Cell Sci 122, 3862–3872.
Moseley JB, Goode BL (2006). The yeast actin cytoskeleton: from cellular function to biochemical mechanism. Microbiol Mol Biol Rev 70, 605–645.
Motegi F, Arai R, Mabuchi I (2001). Identification of two type V myosins in fission yeast, one of which functions in polarized cell growth and moves rapidly in the cell. Mol Biol Cell 12, 1367–1380.
Mulvihill DP, Edwards SR, Hyams JS (2006). A critical role for the type V myosin, Myo52, in septum deposition and cell fission during cytokinesis in *Schizosaccharomyces pombe*. Cell Motil Cytoskeleton 63, 149–161.
Mulvihill DP, Pollard PJ, Win TZ, Hyams JS (2001). Myosin V-mediated vacuole distribution and fusion in fission yeast. Curr Biol 11, 1124–1127.
Nakano K, Imai J, Arai R, Toh EA, Matsui Y, Mabuchi I (2002). The small GTPase Rho3 and the diaphanous/formin For3 function in polarized cell growth in fission yeast. J Cell Sci 115, 4629–4639.
Nambiar R, McConnell RE, Tyska MJ (2010). Myosin motor function: the ins and outs of actin-based membrane protrusions. Cell Mol Life Sci 67, 1239–1254.
Peremyslov VV, Prokhnevsky AI, Dolja VV (2010). Class XI myosins are required for development, cell expansion, and F-actin organization in *Arabidopsis*. Plant Cell 22, 1883–1897.
Reymann AC, Boujemaa-Paterski R, Martiel JL, Guerin C, Cao WX, Chin HF, De La Cruz EM, Thery M, Blanchoin L (2012). Actin network architecture can determine myosin motor activity. Science 336, 1310–1314.
Rincon SA, Ye YF, Villar-Tajadura MA, Santos B, Martin SG, Perez P (2009). Pob1 participates in the Cdc42 regulation of fission yeast actin cytoskeleton. Mol Biol Cell 20, 4390–4399.
Robinson NCG, Guo L, Imai J, Toh-E A, Matsui Y, Tamanoi F (1999). Rho3 of *Saccharomyces cerevisiae*, which regulates the actin cytoskeleton and exocytosis, is a GTPase which interacts with Myo2 and Exo70. Mol Cell Biol 19, 3580–3587.
Rodriguez OC, Schaefer AW, Mandato CA, Forscher P, Bement WM, Waterman-Storer CM (2003). Conserved microtubule-actin interactions in cell movement and morphogenesis. Nat Cell Biol 5, 599–609.
Rossi G, Brennwald P (2011). Yeast homologues of lethal giant larvae and type V myosin cooperate in the regulation of Rab-dependent vesicle clustering and polarized exocytosis. Mol Biol Cell 22, 842–857.
Saarikangas J, Zhao HX, Lappalainen P (2010). Regulation of the actin cytoskeleton-plasma membrane interplay by phosphoinositides. Physiol Rev 90, 259–289.
Scott BJ, Neidt EM, Kovar DR (2011). The functionally distinct fission yeast formins have specific actin-assembly properties. Mol Biol Cell 22, 3826–3839.
Stelter P, Kunze R, Flemming D, Hopfner D, Diepholz M, Philippsen P, Bottcher B, Hurt E (2007). Molecular basis for the functional interaction of dynein light chain with the nuclear-pore complex. Nat Cell Biol 9, 788–796.
Takaine M, Numata O, Nakano K (2009). Fission yeast IQGAP arranges actin filaments into the cytokinetic contractile ring. EMBO J 28, 3117–3131.
Tolic-Norrelykke IM, Sacconi L, Stringari C, Raabe I, Pavone FS (2005). Nuclear and division-plane positioning revealed by optical micromanipulation. Curr Biol 15, 1212–1216.
Tran PT, Marsh L, Doye V, Inoué S, Chang F (2001). A mechanism for nuclear positioning in fission yeast based on microtubule pushing. J Cell Biol 153, 397–411.
Trybus KM (2008). Myosin V from head to tail. Cell Mol Life Sci 65, 1378–1389.
Ueda H, Yokota E, Kutsuna N, Shimada T, Tamura K, Shimmen T, Hasezawa S, Dolja VV, Hara-Nishimura I (2010). Myosin-dependent endoplasmic reticulum motility and F-actin organization in plant cells. Proc Natl Acad Sci USA 107, 6894–6899.
Verde F, Mata J, Nurse P (1995). Fission yeast-cell morphogenesis— identification of new genes and analysis of their role during the cell-cycle. J Cell Biol 131, 1529–1538.
Vidali L, Burkart GM, Augustine RC, Kerdavid E, Tuzel E, Bezanilla M (2010). Myosin XI is essential for tip growth in *Physcomitrella patens*. Plant Cell 22, 1868–1882.
Wagner W, Brenowitz SD, Hammer JA (2011). Myosin-Va transports the endoplasmic reticulum into the dendritic spines of Purkinje neurons. Nat Cell Biol 13, 40–48.
Win TZ, Gachet Y, Mulvihill DP, May KM, Hyams JS (2001). Two type V myosins with non-overlapping functions in the fission yeast *Schizosaccharomyces pombe*: Myo52 is concerned with growth polarity and cytokinesis, Myo51 is a component of the cytokinetic actin ring. J Cell Sci 114, 69–79.
Woolner S, Bement WM (2009). Unconventional myosins acting unconventionally. Trends Cell Biol 19, 245–252.
Yu JH, Crevenna AH, Bettenbuhl M, Freisinger T, Wedlich-Soldner R (2011). Cortical actin dynamics driven by formins and myosin V. J Cell Sci 124, 1533–1541.

Table S1: Strains used in this study

Strain	Genotype	Source
YSM1182	*h+ ade6-M216 leu1-32 ura4-D18*	Lab stock
YSM1532	*h- myo51::ura4+ ade6-M216 leu1-32 ura4-D18*	Lab stock
YSM1923	*h- myo52:.ura4+ leu1-32 ura4-294*	This study
YSM1545	*myo52::ura4+ myo51:ura4+ ade6-M216 leu1-32 ura4-D18*	Lab stock
YSM1537	*h- orb2-34 ura4-D18*	Lab stock
YSM1557	*h- orb6-25 ade6- leu1-32 ura4-D18*	Lab stock
YSM2002	*cdc25-22 myo52::ura4+, myo51::ura4+ leu1-32 ura4-D18*	This study
YSM2003	*cdc25-22 myo51::ura4+ leu1-32 ura4-D18*	This study
YSM1273	*leu1-32::nmt41-GFP-CHD-leu1+ ade6-M216 ura4-D18*	Lab stock
YSM663	*h+ myo51::ura4+ myo52::ura4+ leu1-32::nmt41-GFP-Rng2-CHD-leu1+ ade6-M216 ura4-D18*	Lab stock
YSM423	*h- for3-3GFP-ura4+ ade6-M216 leu1-32 ura4-D18*	Lab stock
YSM439	*for3-3GFP-ura4+ myo51::ura4+ ade6-M216 leu1-32 ura4-D18*	Lab stock
YSM488	*for3-3GFP-ura4+ myo52::ura4+ ade6-M216 leu1-32 ura4-D18*	Lab stock
YSM538	*h+ myo51::ura4+ myo52::ura4+ for3-3GFP-ura4+ ade6-M216 leu1-32 ura4-D18*	Lab stock
YSM2004	*h- myo51-3YFP-KanMX ade6-M216 leu1- 32 ura4-D18 his3-D1*	M. Lord
YSM2005	*h- myo51Δtail-3GFP-ura4+ ade6-M216 leu1-32 ura4-D18*	This study
YSM2006	*for3::KanMX; myo51-3YFP-KanMX ade6-M216 leu1- 32 ura4-D18 his3-D1*	This study
YSM2007	*myo52::ura4+; myo51-3YFP-KanMX ade6-M216 leu1-32 ura4-D18*	This study

YSM2008	*myo51Δtail-3GFP-ura4+ ; myo52::ura4+ ade6-M216 leu1-32 ura4-D18*	This study
YSM2009	*myo51Δtail-3GFP-ura4+; for3::KanMX leu1-32 ura4-D18*	This study
YSM740	*h+ myo52-tdTomato-NatMX ade6-M216 leu1-32 ura4-D18*	Lab stock
YSM2010	*myo51::ura4+; myo52-tdtomatoNatMX leu1-32 ura4-D18-*	This study
YSM2011	*myo52-dtTomato-NatMX; myo51::ura4+; for3::KanMX leu1-32 ura4-D18-*	This study
YSM2012	*myo52Δtail-tdTomato-KanMX; myo51::ura4+; for3-3GFP -ura4+ leu1-32 ura4-D18-*	This study
YSM750	*myo52-dtTomato-NatMX for3-3GFP-ura4+ ade6-M216 leu1-32 ura4-D18*	Lab stock
YSM2013	*myo52Δtail-tdTomato-KanMX; leu1-32 ura4-D18-*	This study
YSM2014	*myo52Δtail-tdTomato-KanMX; myo51::ura4+; leu1-32 ura4-D18-*	This study
YSM2015	*myo51::ura4+; for3::KanMX; myo52Δtail-tdTomato-KanMX; leu1-32 ura4-D18-*	This study
YSM2016	*myo52::ura4;myo51Δtail-12myc-ura4+; for3-3GFP-KanMX leu1-32 ura4-D18*	This study
YSM1925	*h- leu1-32 ura4-294::tea2N-GFP-myo52C-ura4+*	This study
YSM1926	*myo52::ura4+ myo51::ura4+ leu1-32 ura4-294::tea2N-GFP-ura4+*	This study
YSM1927	*myo52::ura4+ myo51::ura4+ leu1-32 ura4-294::GFP-myo52C-ura4+*	This study
YSM1928	*mal3::his3+ myo52::ura4+ myo51::ura4+ leu1-32 ura4-294::tea2N-GFP-myo52C-ura4+*	This study
YSM1929	*myo52::ura4+ myo51::ura4+ leu1-32 ura4-294::tea2N-GFP-myo52C-ura4+*	This study
YSM2017	*myo52::ura4+ myo51::ura4+ leu1-32 ura4-294::tea2N-GFP-myo52C-ura4+ for3-3GFP-*	This study

	KanMX	
YSM2018	*myo52::ura4+ myo51::ura4+ leu1-32::nmt41-GFP-Rng2-CHD-leu1+ ura4-294::tea2N-GFP-myo52C-ura4+*	This study
YSM106	*h- myo52-GFP::kanMX leu1-32 ura4-D18*	Lab stock
YSM107	*for3-4myc::kanMX ade6- leu1-32 ura4-D18*	Lab stock
YSM108	*for3-4myc::kanMX myo52-GFP::kanMX leu1-32 ura4-D18-*	Lab stock
YSM2019	*myo52::ura4; myo51::ura4; ura4-294::8nmt1-myo52motorCC-CFP-ura4+ leu1-32*	This study
YSM2020	*myo51::ura4; myo52::ura4; ura4-294::8nmt1-myo52N-CFP-ura4+; for3-3GFP-KanMX leu1-32*	This study
YSM2021	*ura4-294::8nmt1-myo52N-CFP-nup146-ura4+; myo52::ura4;myo51::ura4 leu1-32*	This study
YSM2022	*ura4-294::8nmt1-myo52N-CFP-nup146-ura4+; myo51::ura4;myo52::ura4; for3-3GFP-KanMX leu1-32*	This study
YSM2023	*myo52::ura4+; ura4-294::8nmt1-myo52m4A-N-CFP-nup146-ura4+ leu1-32*	This study
YSM2024	*myo52::ura4+; ura4-294::8nmt1-myo52m4A-N-CFP-nup146-ura4+; myo51::ura4; for3-3GFP-KanMX leu1-32*	This study
YSM2025	*myo52::ura4; myo51::ura4; leu1-32::nmt41-GFP-Rng2-CHD-leu1+; ura4-294::8nmt1-myo52N-GFP-ura4+*	This study
YSM2026	*myo52::ura4; myo51::ura4; leu1-32::nmt41-GFP-Rng2-CHD-leu1+; ura4-294::8nmt1-myo52N-GFP-nup146-ura4+*	This study
YSM2027	*myo51-3YFP-KanMX; for3::KanMX; Crn1-tdTomato-NatMX leu1-32 ura4-D18*	This study
YSM2028	*ypt3-i5 (ts); myo51::ura4; leu1-32::nmt41-GFP-Rng2-CHD-leu1+*	This study

YSM2029	*myo51::ura4; myo52Tomato-NatMX;ypt3-i5 (ts) leu1-32*	This study
YSM2030	*myo52::ura4+; myo51::ura4+; bud6-3GFP-KanMX6 leu1-32 ura4-D18*	This study
YSM2031	*myo52::ura4+; myo51::ura4+; leu1-32 ura4-294::shk1 promoter:ScGIC2 CRIB:GFP3:ura4+*	This study
YSM2032	*myo52::ura4+;myo51::ura4+;pob1-GFP-ura4+ leu1-32 ura4-D18*	This study
YSM2033	*myo52::ura4+; myo51::ura4+; tip1-GFP-KanMX leu1-32 ura4-D18*	This study
YSM2034	*myo52::ura4+; myo51::ura4+; tea4 GFP-KanMX leu1-32 ura4-D18*	This study
YSM1089	*nup107-td-Tomato-NatMX ade6-M216 leu1-32 ura4-D18*	Lab stock
YSM2106	*myo52-GFP-KanMX leu1-32 ura4-D18 [Rep41-tomato-ypt3-leu+]*	This study
YSM2107	*myo52::ura4+, myo51::ura4+; ura4-294-myo52N-GFP-nup146-ura4+ leu1-32 [Rep41-tomato-ypt3-leu+]*	This study
YSM2066	*nup107-tdTomato-NatMX; ura4-294::8nmt1-myo52N-GFP-nup146-ura4+ leu1-32*	This study
YM1085	*h- mal3::his3+ ade6-M210 leu1-32 ura4-D18*	Lab stock
YSM2157	*myo52::ura4+ myo51::ura4+mal3::his3+ leu1-32 ura4-D18*	This study

Figure S1. Pharmacological or genetic disruption of microtubules exacerbates the cable defect of *myoV*Δ cells.

A. Alexafluor-phalloidin staining of *myoV*+ (left panels) and *myoV*Δ cells (right panels) untreated (top panels), treated with 25µg/ml MBC for 30min (middle panels) or lacking *mal3* (bottom panels). Arrowheads point to thick cable. **B** and **C.** Quantifications of the actin defect as assessed in A. Scale bars represent 5µm.

Figure S2. Full-length versus truncated type-V myosins: more on drug sensitivity, localization and expression levels.

A. Cells expressing either Myo51-3YFP (left panel) or Myo51Δtail-3GFP (right panel) after 10 minutes treatment with 10µM LatA. **B.** Two color image of *for3*Δ cells expressing Myo51-3YFP (shown in green) and the actin patch marker Crn1-tdTomato (shown in red). **C.** Quantification of fluorescence intensities of endogenously expressed truncated Myo52Δtail-tdTomato relative to endogenously expressed full-length Myo52-tdTomato in wild type and *myo51*Δ backgrounds. Error bars show the standard deviation. Scale bars represent 5µm.

Figure S3. Functional inactivation of Ypt3p, a cargo receptor for Myo52, weakly mimics the cable defect of *myoV*Δ cells.

A. Alexafluor-phalloidin staining of *myo51*Δ and *myo51*Δ *ypt3-i5* cells at 25ºC. **B.** Actin organization in live cells expressing the actin marker GFP-CHD_{Rng2} at 25°C. **C.** Quantification of the actin defect in (A)**. D.** Tip-localization of Myo52-tdTomato in *myo51*Δ (left panels) and *myo51*Δ *ypt3-i5* cells (right panels) at the permissive (25°) (top panels) and restrictive temperature (36°) (bottom panels). Scale bars represent 5 µm.

Figure S4. The localization to cell tips of known actin cable regulators is unaffected in *myoV*Δ cells.

Maximum projection of spinning disk confocal images of wild type (left) and *myoV*Δ (right) cells expressing CRIB-GFP (A), Bud6-3GFP (B), Pob1-GFP (C), Tea4-GFP (D) and Tip1-GFP (E). Scale bar represents 5 µm.

Lo Presti et al, Figure S1

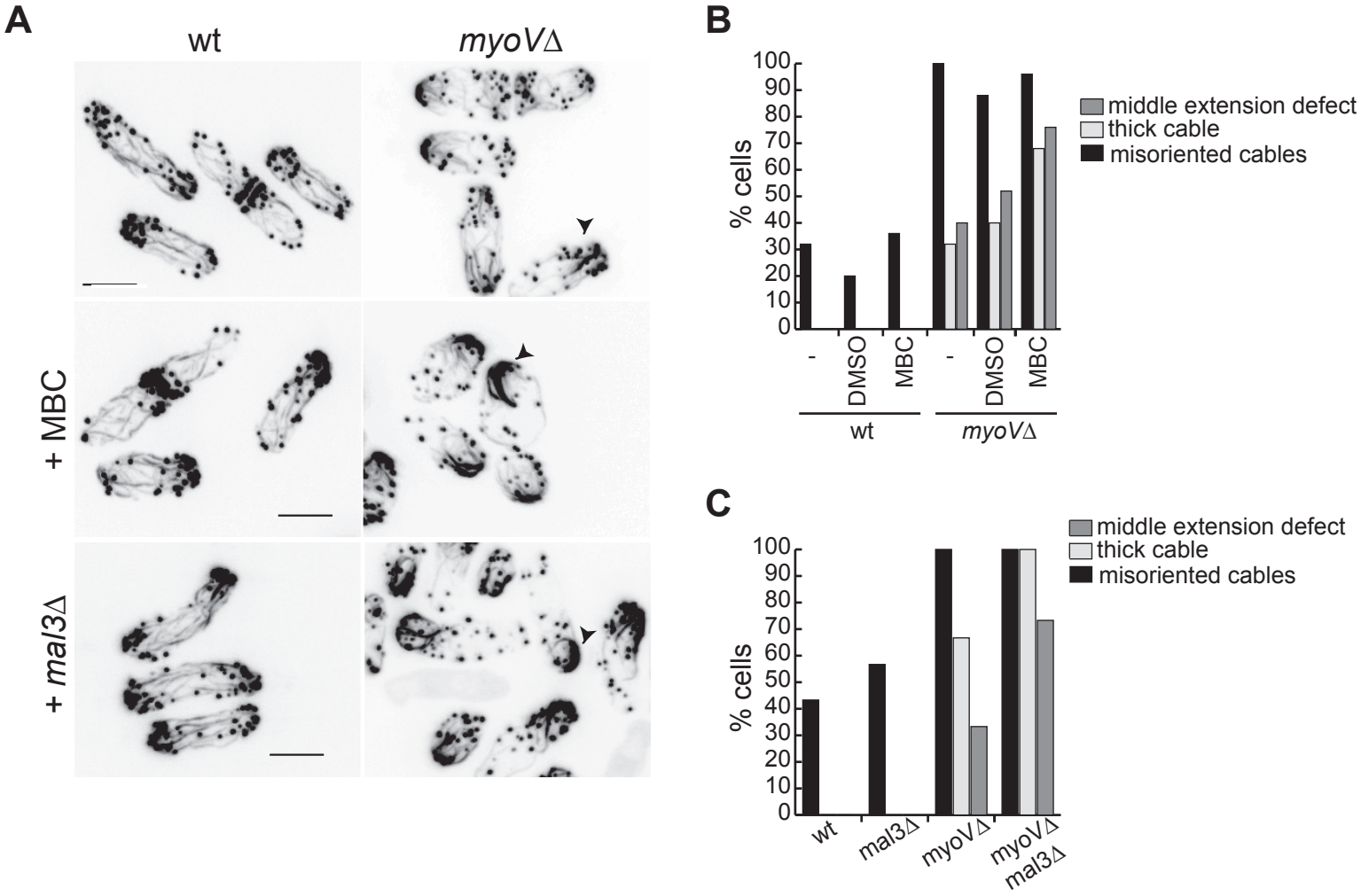

Lo Presti et al, Figure S2

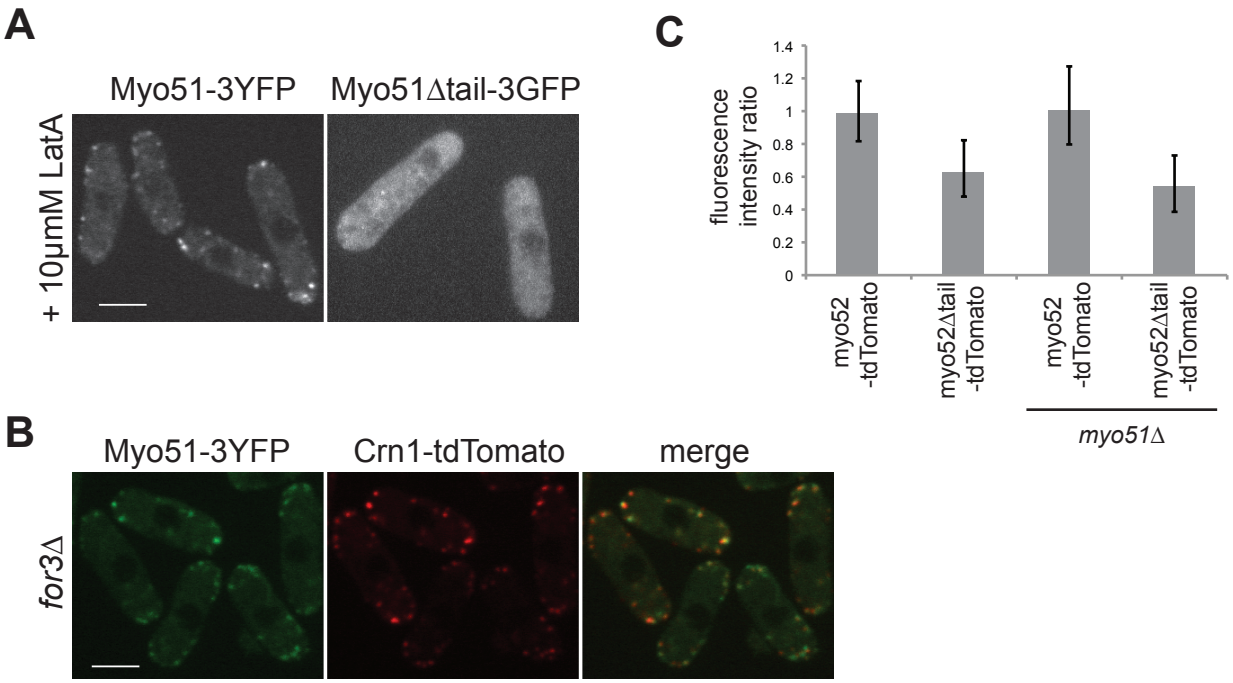

Lo Presti et al, Figure S3

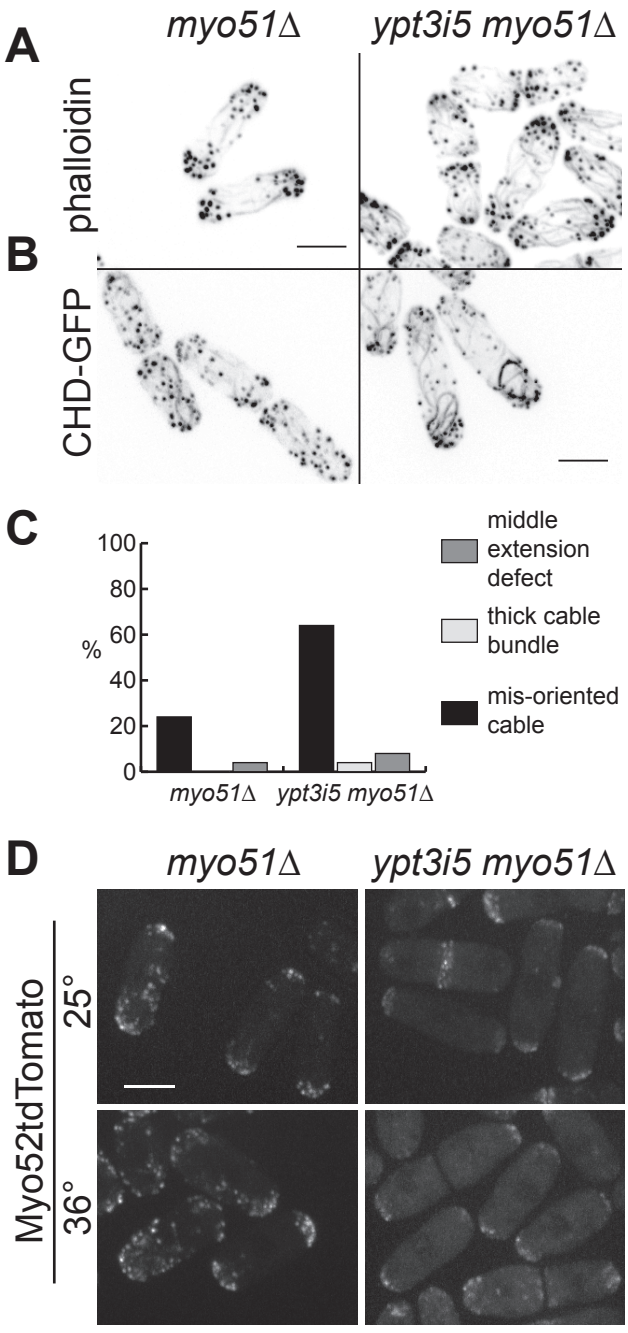

Lo Presti et al, Figure S4